Evaluation of Precipitation Simulated by Seven SCMs against the ARM Observations at the SGP Site*

HUA SONG,[+] WUYIN LIN,[+] YANLUAN LIN,[#,++] AUDREY B. WOLF,[@] ROEL NEGGERS,[&] LEO J. DONNER,[#] ANTHONY D. DEL GENIO,[**] AND YANGANG LIU[+]

[+] *Brookhaven National Laboratory, Upton, New York*
[#] *NOAA/Geophysical Fluid Dynamics Laboratory, Princeton, New Jersey*
[@] *Columbia University, New York, New York*
[&] *Royal Netherlands Meteorological Institute, De Bilt, Netherlands*
[**] *NASA Goddard Institute for Space Studies, New York, New York*

(Manuscript received 9 May 2012, in final form 2 January 2013)

ABSTRACT

This study evaluates the performances of seven single-column models (SCMs) by comparing simulated surface precipitation with observations at the Atmospheric Radiation Measurement Program Southern Great Plains (SGP) site from January 1999 to December 2001. Results show that although most SCMs can reproduce the observed precipitation reasonably well, there are significant and interesting differences in their details. In the cold season, the model–observation differences in the frequency and mean intensity of rain events tend to compensate each other for most SCMs. In the warm season, most SCMs produce more rain events in daytime than in nighttime, whereas the observations have more rain events in nighttime. The mean intensities of rain events in these SCMs are much stronger in daytime, but weaker in nighttime, than the observations. The higher frequency of rain events during warm-season daytime in most SCMs is related to the fact that most SCMs produce a spurious precipitation peak around the regime of weak vertical motions but rich in moisture content. The models also show distinct biases between nighttime and daytime in simulating significant rain events. In nighttime, all the SCMs have a lower frequency of moderate-to-strong rain events than the observations for both seasons. In daytime, most SCMs have a higher frequency of moderate-to-strong rain events than the observations, especially in the warm season. Further analysis reveals distinct meteorological backgrounds for large underestimation and overestimation events. The former occur in the strong ascending regimes with negative low-level horizontal heat and moisture advection, whereas the latter occur in the weak or moderate ascending regimes with positive low-level horizontal heat and moisture advection.

1. Introduction

Precipitation is one of the most poorly parameterized physical processes in numerical weather prediction and general circulation models (GCMs). While the double intertropical convergence zone (ITCZ) phenomenon is probably the most outstanding problem confronting GCMs for properly simulating precipitation climatology (Lin 2007), there are long-standing challenges for GCMs to simulate precipitation features as fundamental as the diurnal variation, and the frequency and intensity associated with individual weather systems. For example, most GCMs exhibit substantial biases in simulating the diurnal cycle of warm-season precipitation, producing too much precipitation in daytime but too little precipitation in nighttime over land, and wrong timing of convective precipitation events in general (e.g., Ghan et al. 1996; Dai 2006; Lee et al. 2007; Lee and Schubert 2008). It is also common that models substantially overestimate the frequency of light precipitation and underestimate the intensity and/or frequency of heavy precipitation (e.g., Dai and Trenberth 2004; Sun et al. 2006). Even

* Supplemental information related to this paper is available at the Journals Online website: http://dx.doi.org/10.1175/JCLI-D-00263.s1.

[++] Current affiliation: Ministry of Education Key Laboratory for Earth System Modeling, Center for Earth System Science, Tsinghua University, Beijing, China.

Corresponding author address: Hua Song, Atmospheric Sciences Division, Brookhaven National Laboratory, 75 Rutherford Dr., Bldg. 815E, Upton, NY 11973-5000.
E-mail: hsong@bnl.gov

DOI: 10.1175/JCLI-D-12-00263.1

© 2013 American Meteorological Society

without considering the inevitable influence on the atmospheric circulation, the sheer bias in simulating the probability distribution of precipitation should cast doubt on the model's capability to predict high-impact hydrological events.

One of the difficulties with modeling precipitation stems from the fact that in addition to large-scale circulation, precipitation is affected by a variety of complex processes that need to be parameterized in large-scale models, for example, deep convection, planetary boundary layer processes, and cloud microphysics (Dai 2006). It is not trivial to identify deficient aspects of the parameterizations, and many approaches have been proposed for this purpose. One of the commonly used approaches is to perform and evaluate simulations of corresponding single-column models (SCMs) driven by the same large-scale forcing (e.g., Randall et al. 2003; Neggers et al. 2012).

The SCM approach is also a key strategy of the U.S. Department of Energy's Atmospheric Radiation Measurement (ARM) and Atmospheric System Research (ASR) programs (Stokes and Schwartz 1994; Ackerman and Stokes 2003). ARM organized several SCM intercomparisons using surface observations at the ARM sites. However, most of the previous studies have been focused on special cases, or week-to-month-long periods (e.g., Ghan et al. 2000; Xie et al. 2002, 2005). The scopes of such studies are often limited by the availability of large-scale forcing needed to drive the SCM simulations. Xie et al. (2004) have constructed multiyear (1999–2001) continuous large-scale forcing data over the Southern Great Plains (SGP) site using an objective variational analysis method constrained by surface and top-of-the-atmosphere (TOA) observations. Together with other observations, the multiyear continuous large-scale forcing data permit long-term SCM-based evaluation of the parameterized physics with much improved statistics. Kennedy et al. (2010) have lately evaluated the Goddard Institute for Space Studies (GISS) SCM-simulated clouds by taking advantage of the 3-yr large-scale forcing data. Driven by these observationally constrained continuous large-scale forcing data, we have further carried out 3-yr (1999–2001) SCM simulations of seven GCMs participating in the Fast-Physics System Testbed and Research (FASTER) project at the ARM SGP site, with the aid of the FASTER SCM testbed. (Detailed information on the FASTER project and the testbed can be found at http://www.bnl.gov/faster/.)

This study focuses on the statistical aspects that bear relevance to main existing issues of precipitation simulation (e.g., diurnal cycle, seasonal variation, and convective/stratiform partitioning), including differing model biases in frequency and mean precipitation intensity between daytime and nighttime, between warm and cold seasons, and between convective and stratiform partition. In addition, we also attempt to demonstrate the relationship between surface precipitation and vertical-pressure velocity, precipitable water, and relative humidity, and to investigate the large-scale backgrounds against which the model biases occur through the studies of extreme events.

The rest of the paper is organized as follows: section 2 describes the model and data used in this study. The main results are presented in sections 3 and 4. Section 5 summarizes the major results.

2. Model description and evaluation data

a. Participating models

Three main U.S. GCMs—the Community Atmosphere Model (CAM), the Geophysical Fluid Dynamics Laboratory (GFDL) Atmospheric Model (AM), and the GISS Model E2—and one European GCM—the European Centre for Medium-Range Weather Forecasts (ECMWF) Integrated Forecast System (IFS)—participate in the FASTER project. To further enhance the parameterization diagnosis and track the model improvement, the CAM and GFDL AM also include multiple versions (CAM, versions 3, 4, and 5; GFDL AM, versions 2 and 3). Note that the GFDL AM3 here is not the full version of GFDL AM3 (Donner et al. 2011), which uses 48 vertical levels with aerosol activation (double moment for cloud droplets) and comprehensive chemistry. The AM3 here is close to the AM2 with the same vertical levels and cloud scheme. The major change of the AM3 from the AM2 is the convection scheme. The AM2 uses the relaxed Arakawa–Schubert scheme (Moorthi and Suarez 1992) for both deep and shallow convections, while the AM3 uses the Donner cumulus scheme (Donner et al. 2001, 2011) for deep convection and University of Washington (UW) scheme (Bretherton et al. 2004a; Zhao et al. 2009) for shallow convection.

Table 1 lists the seven GCMs used in the intercomparison study, their precipitation-related parameterization schemes, the corresponding references, and their SCM vertical and temporal resolutions. All the deep convection schemes of the seven GCMs are based on the mass-flux approach, with differences in their closure assumptions, trigger mechanisms, and formulations for convective updrafts and downdrafts. Previous studies show that the deficiency in the convective trigger mechanism is one of the major reasons for different timing of precipitation occurrences (e.g., Xie and Zhang 2000; Betts and Jakob 2002; Zhang 2003; Bechtold et al. 2004; Lee et al. 2008). There are four kinds of convection triggers in the seven GCMs: convective available potential energy (CAPE) threshold triggers for the GFDL

TABLE 1. Participating SCMs and related parameterizations, where AS is Arakawa and Schubert (1974) and ZM is Zhang and McFarlane (1995). The single-column version of GISS-E2 uses a 1-moment cloud microphysics scheme, while the full GISS-E2 uses a 2-moment microphysics scheme. Also, the implementation of the deep cumulus parameterization in GFDL AM3 differs from Donner et al. (2001), as described in Donner et al. (2011). Finally, the single-column version of AM3 differs from the GCM described in Donner et al. (2011) by using a specified droplet concentration of 300 cm^{-3} instead of interactive aerosols and chemistry.

Model	Convection scheme	Cloud scheme	PBL	Resolution	
				Levels	Minutes
GISS-E2	Bulk mass flux, deep and shallow (Del Genio and Yao 1993; Del Genio et al. 2007) and cumulus microphysics (Del Genio et al. 2005)	Micro/macrophysics (Del Genio et al. 1996; Schmidt et al. 2006; G. A. Schmidt et al. 2012, unpublished manuscript)	Local TKE and counter gradient (Schmidt et al. 2006)	40	30
GFDL AM2	Relaxed AS, deep and shallow (Moorthi and Suarez 1992)	1-moment microphysics (Rotstayn 1997) and cloud macrophysics (Tiedtke 1993)	K-profile scheme (Lock et al. 2000)	24	30
GFDL AM3	Donner, deep (Donner et al. 2001, 2011) and UW, shallow (Zhao et al. 2009)	1-moment microphysics (Rotstayn 1997) and cloud macrophysics (Tiedtke 1993)	K-profile scheme (Lock et al. 2000)	24	30
ECMWF IFS	Bulk mass flux, deep and shallow (Tiedtke 1989; Gregory et al. 2000)	1-moment microphysics and cloud macrophysics (Tiedtke 1993; Gregory et al. 2000)	Eddy-diffusivity/mass-flux scheme (Köhler 2005)	91	5
CAM3	Simplified AS, deep (Zhang and McFarlane 1995) and Hack, shallow (Hack 1994)	1-moment microphysics (Rasch and Kristjansson 1998) and cloud macrophysics (Zhang et al. 2003)	Non-local K-profile scheme (Holtslag and Boville 1993)	26	20
CAM4	Modified ZM, deep (Neale et al. 2008) and Hack, shallow (Hack 1994)	1-moment microphysics (Rasch and Kristjansson 1998) and cloud macrophysics (Zhang et al. 2003)	Non-local K-profile scheme (Holtslag and Boville 1993)	26	20
CAM5	Modified ZM, deep (Neale et al. 2008) and UW, shallow (Park and Bretherton 2009)	2-moment microphysics (Morrison and Gettelman 2008) and cloud macrophysics (S. Park et al. 2010, unpublished manuscript)	UW diagnostic TKE (Bretherton and Park 2009)	30	20

AM3 and CAM3, cloud work function threshold triggers for the GFDL AM2, dilute CAPE threshold triggers for the CAM4 and CAM5, and parcel-lifting-based triggers for the GISS-E2 and ECMWF models. Dilute CAPE and cloud work function for entraining clouds are closely related, though the quantitative values of entrainment may vary widely. The SCM intercomparison study of Xie et al. (2002) indicates that the models using CAPE-only triggers generally produce the least agreement with the observations in surface precipitation. The planetary boundary layer (PBL) schemes also differ among the models. The CAM3 and CAM4 use a dry and surface-driven PBL scheme and produce a very shallow PBL, while the ECMWF model uses an eddy-diffusivity/mass-flux approach and produces a deeper and better mixed PBL (Hannay et al. 2009). More information on the parameterization schemes can be found in the related references given in Table 1.

b. Model configuration and setup

The basic thermodynamic configuration for the SCM consists of two prognostic equations about temperature T and specific humidity q:

$$\frac{\partial \overline{T}(p,t)}{\partial t} = -\overline{\boldsymbol{v}} \cdot \nabla \overline{T} - \overline{\omega}\frac{\partial \overline{T}}{\partial p} + \frac{\overline{\omega}}{c_p}\alpha + P_T + \frac{\overline{T}_{\rm obs} - \overline{T}}{\tau_a} \quad \text{and}$$

$$\frac{\partial \overline{q}(p,t)}{\partial t} = -\overline{\boldsymbol{v}} \cdot \nabla \overline{q} - \overline{\omega}\frac{\partial \overline{q}}{\partial p} + P_q + \frac{\overline{q}_{\rm obs} - \overline{q}}{\tau_a},$$

where the overbar denotes the large (model grid)-scale mean, $\overline{\boldsymbol{v}}$ is the large-scale horizontal wind velocity, $\overline{\omega}$ is the large-scale vertical pressure velocity, $-\overline{\boldsymbol{v}} \cdot \nabla \overline{T}$ and $-\overline{\boldsymbol{v}} \cdot \nabla \overline{q}$ are the large-scale horizontal advection tendencies, $-\overline{\omega}(\partial \overline{T}/\partial p)$ and $-\overline{\omega}(\partial \overline{q}/\partial p)$ are the large-scale vertical advection tendencies, and α is the specific volume. Here, P_T and P_q are the parameterized physics tendencies and $(\overline{T}_{\rm obs} - \overline{T})/\tau_a$ and $(\overline{q}_{\rm obs} - \overline{q})/\tau_a$ are the relaxation terms, with $\overline{T}_{\rm obs}$ and $\overline{q}_{\rm obs}$ being the observed values of T and q respectively, and τ_a being the relaxation time scale, which is set to 3 h based on previous studies (e.g., Hack and Pedretti 2000).

Since SCMs do not predict the interaction with the environment outside of the target column, nor do they predict the vertical motion within the column, both the large-scale horizontal and vertical advection tendencies, along with surface forcings, are prescribed using the

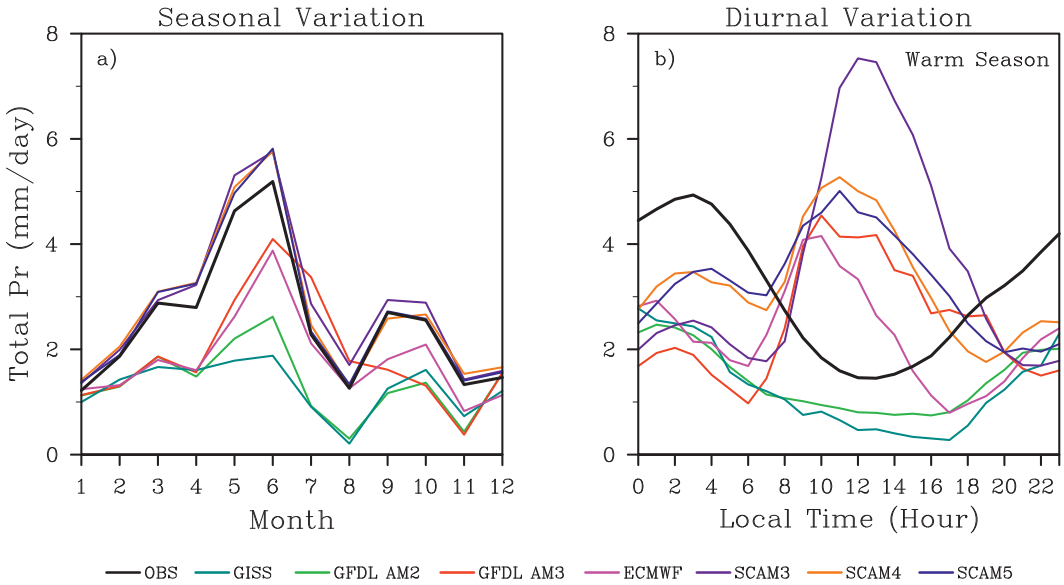

FIG. 1. (a) Seasonal and (b) warm-season diurnal variations of total precipitation (Pr) in observations and 7 SCMs averaged for years 1999–2001. Note that GISS refers to model GISS-E2 (here and in subsequent figures).

ARM variational analysis product (Xie et al. 2004). The variational analysis product was generated by constraining the National Oceanic and Atmospheric Administration (NOAA) Rapid Update Cycle, version 2 (RUC-2), analyses with ARM surface and TOA measurements.

The relaxation terms relax the simulated T and q toward the observations at each time step. They are unphysical and may appear to hide the errors in model physics (Ghan et al. 1999). However, Randall and Cripe (1999) found that error in SCM is conserved and the use of relaxation does not hide model problems. Relaxation can also suppress the model's sensitivity to initial condition (Hack and Pedretti 2000) and act to adaptively correct the error in large-scale forcing. Precipitation in SCM is strongly constrained by the forcing. When the SCM is simply forced with the continuous large-scale forcing, the simulated precipitation cannot stray too far from the observed precipitation, even when the model's thermodynamic state has large accumulated biases (e.g., Randall and Cripe 1999; Hack and Pedretti 2000). This would render the SCM framework ineffective in evaluating the underlying precipitation physics. Use of relaxation under such circumstances serves to unlock the strong link between large-scale forcing and precipitation.

For the 3-yr simulations from January 1999 to December 2001, all seven SCMs are reinitialized at the beginning of each month and integrated for each whole month. The seven SCM outputs are averaged over 1 h to match the temporal resolution of evaluation data (see Table 1 for the original SCM temporal resolutions).

c. *Evaluation data*

The precipitation data used in this study for evaluation are the SGP domain-averaged surface precipitation rates included in the continuous forcing data derived by Xie et al. (2004). They are the hourly Arkansas–Red Basin River Forecast Center (ABRFC) 4-km rain gauge–adjusted Weather Surveillance Radar-1988 Doppler (WSR-88D) measurements averaged over the variational analysis domain.

Fields of vertical pressure velocity, specific humidity, relative humidity, horizontal thermal advection, horizontal moisture advection, surface latent heat (LH) flux, and sensible heat (SH) flux in the continuous large-scale forcing data (Xie et al. 2004) are also used in this study.

3. Results

a. *Seasonal and diurnal variations of precipitation*

Precipitation at the SGP site has strong seasonal and diurnal variations. For the seasonal variation (Fig. 1a), all seven SCMs can reproduce the bimodal pattern in the observations, with the primary peak precipitation in June, the secondary peak precipitation between September and October, and a minimum precipitation in August and between November and January for years 1999–2001. The precipitation rates in the three single-column atmosphere models (SCAMs) are quite close to the observations during all the seasons, while those in the GISS-E2 and GFDL AM2 SCMs are much smaller than the observations, especially during the warm season

TABLE 2. Summary of relative differences of mean intensity M, std dev S, correlation coefficient C, and relative Euclidean distance D between the 7 SCMs and observations of precipitation for all season, warm season, and cold season during years 1999–2001. Equations used to calculate the variables are provided at the bottom of the table.

		SCM						
Season	Variable	GISS-E2	GFDL AM2	GFDL AM3	ECMWF IFS	CAM3	CAM4	CAM5
All	M	−0.49	−0.46	−0.21	−0.28	0.13	0.09	0.07
	S	−0.24	−0.30	−0.15	−0.20	−0.05	−0.08	−0.04
	C	0.20	0.17	0.34	0.25	0.40	0.21	0.25
	D	0.59	0.57	0.43	0.41	0.42	0.24	0.26
Warm	M	−0.59	−0.54	−0.15	−0.26	0.15	0.06	0.06
	S	−0.29	−0.42	−0.18	−0.22	−0.04	−0.12	−0.08
	C	0.24	0.16	0.46	0.34	0.52	0.28	0.32
	D	0.70	0.70	0.52	0.48	0.54	0.31	0.34
Cold	M	−0.34	−0.33	−0.32	−0.31	0.08	0.13	0.09
	S	−0.15	−0.10	−0.09	−0.17	−0.07	−0.001	0.01
	C	0.14	0.14	0.15	0.09	0.18	0.10	0.12
	D	0.40	0.37	0.37	0.37	0.21	0.16	0.15

$$M = \frac{\text{mean}\,(\text{Pr}_{\text{SCM}}) - \text{mean}\,(\text{Pr}_{\text{obs}})}{\text{mean}\,(\text{Pr}_{\text{obs}})} \qquad C = 1 - \text{cor}\,(\text{Pr}_{\text{SCM}}, \text{Pr}_{\text{obs}})$$

$$S = \frac{\text{std dev}\,(\text{Pr}_{\text{SCM}}) - \text{std dev}\,(\text{Pr}_{\text{obs}})}{\text{std dev}\,(\text{Pr}_{\text{obs}})} \qquad D = \sqrt{M^2 + S^2 + C^2}$$

from May to October. Note that the monthly mean precipitation rate in the GISS-E2 SCM shown in Fig. 1a is different from that in Kennedy (2011), which can largely be explained by the difference in the simulation setups. The GISS-E2 SCM simulations in Kennedy (2011) were forced by the continuous forcing without relaxation, whereas the simulations here include the relaxation of temperature and specific humidity. The relaxation tends to produce a net drying of the PBL, and thereby leads to a decreased precipitation rate.

For the diurnal variation in the warm season (Fig. 1b), the maximum precipitation rate in the observations occurs around 0200 LT (SGP local time = UTC − 6 hours) and the minimum occurs around noon. Only the GISS-E2 and GFDL AM2 SCMs can reproduce the observed diurnal phases, although the amplitude is only about half of the observed. The other SCMs do produce a weak peak around the time of the observed maximum, but more noticeable is the spurious peak near noontime. Their mean magnitude of diurnal variation is, however, comparable to the observed, except for the CAM3 SCM. The existence of the spurious noontime precipitation peak, as seen in Fig. 1b, is similar to many previous studies (e.g., Xie and Zhang 2000; Betts and Jakob 2002; Zhang 2003; Bechtold et al. 2004; Lee and Schubert 2008).

The contrasting performances of different models in simulating the phase and magnitude of warm-season diurnal variation are further substantiated in Table 2, which summarizes the relative differences of mean intensity, standard deviation, and correlation coefficient, and the relative Euclidean distance between the seven SCMs and observed precipitation for all seasons, the warm season (May–October), and the cold season (November–April) respectively in years 1999–2001. Relative Euclidean distance is a nondimensional measure gauging the overall agreement between two sets of data in terms of their mean, standard deviation, and correlation coefficient, with zero indicating a perfect agreement between the model and observations and increasing as the agreement degrades (Wu et al. 2012; Liu et al. 2013). Table 2 confirms that the overall performance (relative Euclidean distance) of different models may have very different reasons. For example, the main contributors to the disagreement with observations are the mean bias for the GISS-E2 and GFDL AM2 SCMs (too weak precipitation intensity), but are the poor correlation coefficients (wrong phase) for the three CAM SCMs (hereafter referred to as SCAM3, SCAM4, and SCAM5, respectively). Furthermore, all the SCMs perform much better in the cold than warm season, and all the SCMs (except for SCAM5 in the cold season) underestimate the variability of precipitation compared to the observation.

Preceding results indicate that different models likely perform differently under different conditions. Next we will further investigate the model performances under different conditions by analyzing the contrast of precipitation characteristics between daytime and nighttime and between the cold and warm seasons. The results will also indirectly expose the differences in underlying physical parameterizations of the different SCMs responsible for the simulated precipitation diurnal variations.

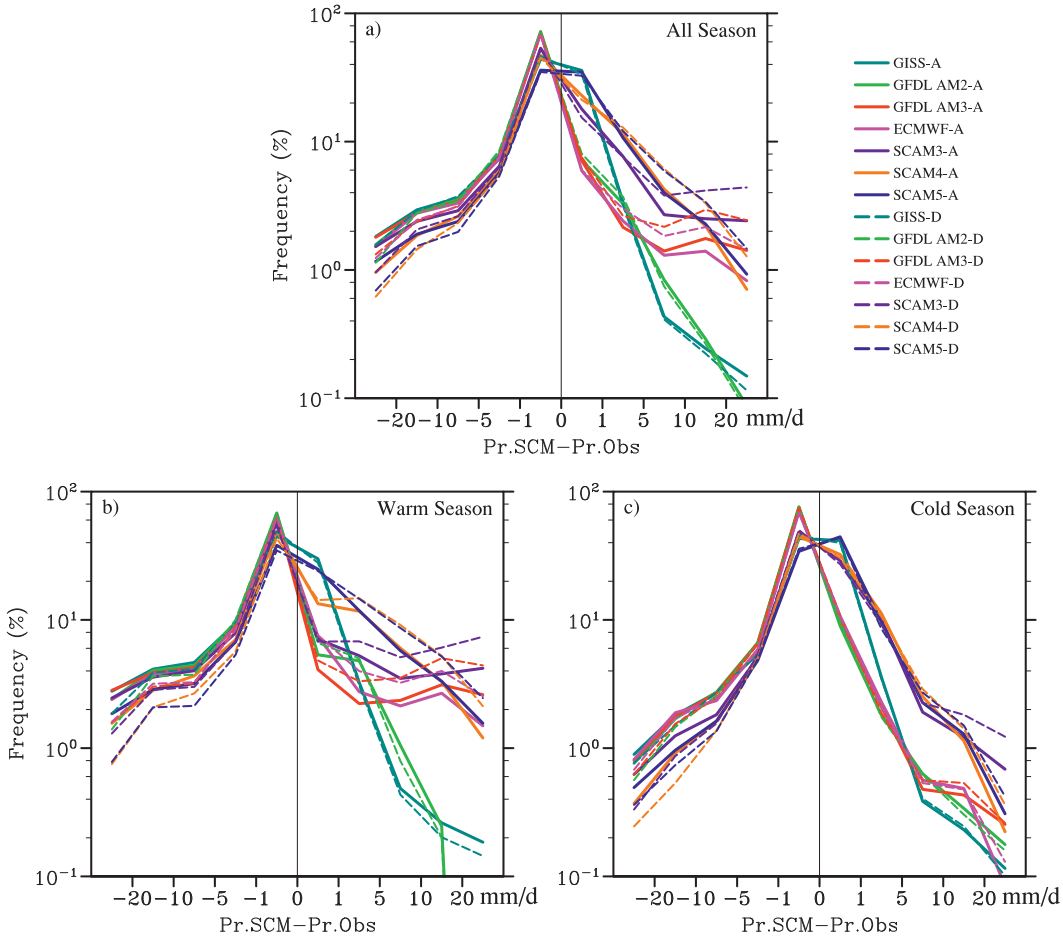

FIG. 2. Frequency of specified model biases in total precipitation for all-time (solid lines) and daytime-only (dashed lines) data for (a) all season, (b) warm season, and (c) cold season.

b. *Frequency distribution of model biases*

To investigate the capability of SCMs to reproduce the observed precipitation at different precipitation intensities, we first analyze the difference of precipitation intensity between the SCMs and observation.

Figure 2a shows the frequency distribution of the model–observation differences in total precipitation intensity for all-time and daytime data, respectively. The frequency distribution for the nighttime data can be inferred from the all-time and daytime patterns. Here, daytime is defined as solar insolation at TOA being larger than 0.01 W m^{-2} (otherwise nighttime). Several points are evident. First, the absolute model biases are mostly less than 1 mm day^{-1}, with the total frequency about 70% and above (Table 3). Second, the SCMs

TABLE 3. The total frequency (%) of events with |model bias| < 1 mm day^{-1} and |model bias| > 10 mm day^{-1} during years 1999–2001 in 7 SCMs. Model bias is the precipitation rate in SCM minus precipitation rate in observations.

		Model events						
Season	|Bias| (mm d^{-1})	GISS-E2	GFDL AM2	GFDL AM3	ECMWF IFS	CAM3	CAM4	CAM5
All	<1	79.96	79.55	77.59	76.33	71.46	69.94	70.93
	>10	5.15	4.79	7.76	6.51	8.84	5.72	6.27
Warm	<1	74.89	73.51	69.85	71.67	65.30	62.73	62.93
	>10	7.35	6.69	12.42	10.36	14.03	8.90	9.61
Cold	<1	84.67	85.21	84.93	80.31	77.25	76.97	78.66
	>10	3.05	2.97	3.25	3.27	3.77	2.65	3.05

underestimate the observed precipitation intensity more frequently than they overestimate. Third, while the frequencies of having large negative biases are comparable among the models, the likelihood of having large positive biases is much more distinguishable. Finally, large positive biases much more frequently happen in the daytime than in the nighttime, except for the GISS-E2 and GFDL AM2 SCMs, which have much fewer large overestimation events anyway.

The frequency distribution of the model biases in precipitation intensity for the warm and cold seasons are shown in Figs. 2b and 2c, respectively. It is seen that the frequencies of large precipitation biases, especially daytime overestimation events, are much higher in the warm than cold season, implying that most SCMs perform better in the cold than warm season. Again, there are very few overestimation events in the GISS-E2 and GFDL AM2 SCMs for both the warm and cold seasons. Figure 2b and Table 3 also reveal that the discrepancy in frequency of large positive biases among the models as seen in Fig. 2a happens in the warm season.

The above analyses show that although all seven SCMs can produce the observed precipitation reasonably well [more than 70% of the time the models have very small biases, and large model biases occur only less than 10% of the time (Table 3)], they tend to underestimate the observed precipitation intensity more frequently than they overestimate, with more striking model differences between the daytime and nighttime and between warm and cold seasons.

c. *Frequency versus intensity analyses*

The total precipitation amount during a period can be expressed as a product of the number of all precipitation events and the mean precipitation intensity of all precipitation events during that period. Similarly, the bias in model precipitation may be attributed to biases in precipitation intensity and/or frequency of precipitation events. This section examines the SCM performance from this perspective. Bias analysis of precipitation intensity and/or frequency may also shed light on deficiencies in the treatment of the underlying physical processes, particularly the relative roles of convective and stratiform precipitating processes in contributing to the total precipitation and its biases. It is noteworthy that while it is well known that GCMs (e.g., Dai and Trenberth 2004) tend to overestimate the frequency of light precipitation and underestimate the frequency of heavy precipitation, in those unconstrained model simulations the difference in simulated frequency occurrence of precipitating weather regimes and their maintenances could also be an important factor. Use of SCMs driven by the same observed large-scale forcings in this study minimizes the influences of potential biases from large-scale atmospheric and surface conditions.

Figure 3 compares the frequency of occurrence and mean intensity of rain events in the seven SCMs and observations for all season, warm season, and cold season. Here, a rain event is defined by the hourly surface total precipitation intensity larger than 0.1 mm day^{-1}, and frequency is the ratio of the number of rain events to the total number of samples. In the observations, rain occurs about 28% of the time in both daytime and nighttime (Fig. 3a). Compared with the observations, the three SCAMs produce more rain events while the two GFDL AM and ECMWF SCMs produce much fewer rain events. Except for the GISS-E2 SCM, the other six SCMs rain more frequently in the daytime than in the nighttime. Yet the mean hourly precipitation intensities in most SCMs are weaker than the observed, especially in the nighttime. The observed mean precipitation intensity is stronger in the nighttime than in the daytime, which is opposite in the GFDL AM3 and three SCAMs. The distributions of frequency and mean intensity of rain events in the warm and cold seasons are quite different. In the warm season (Fig. 3b), the three SCAMs have more rain events than the observations in the daytime, but most SCMs have fewer rain events than the observations in the nighttime. Among the three SCAMs, nighttime precipitation frequency improves from SCAM3 to SCAM4 and SCAM5, but the daytime overestimated precipitation frequency is biased further higher. In general among the SCAMs, the higher the precipitation frequency a model has, the lower the mean precipitation intensity, suggesting some compensating errors between precipitation intensity and frequency in the SCAMs. The GISS-E2 and GFDL AM2 SCMs tend to underestimate frequency and intensity in both daytime and nighttime, while the GFDL AM3 and ECMWF SCMs underestimate the frequency but overestimate the mean intensity in both daytime and nighttime. In the cold season (Fig. 3c), the GISS-E2 SCM and three SCAMs have higher precipitation frequency but weaker precipitation intensity relative to the observations, which is true for both daytime and nighttime conditions. The two GFDL and ECMWF SCMs have much lower frequency but stronger intensity than the observations in daytime.

The existence of compensating errors between precipitation frequency and mean intensity becomes more evident in Fig. 4, which shows the relationship between the relative differences in precipitation frequency and mean intensity for all season (Fig. 4a), warm season (Fig. 4b), cold season (Fig. 4c), and those with an absolute value of model precipitation bias less than 5 mm day^{-1} (Fig. 4d). The diagonal line is indicative of perfect error

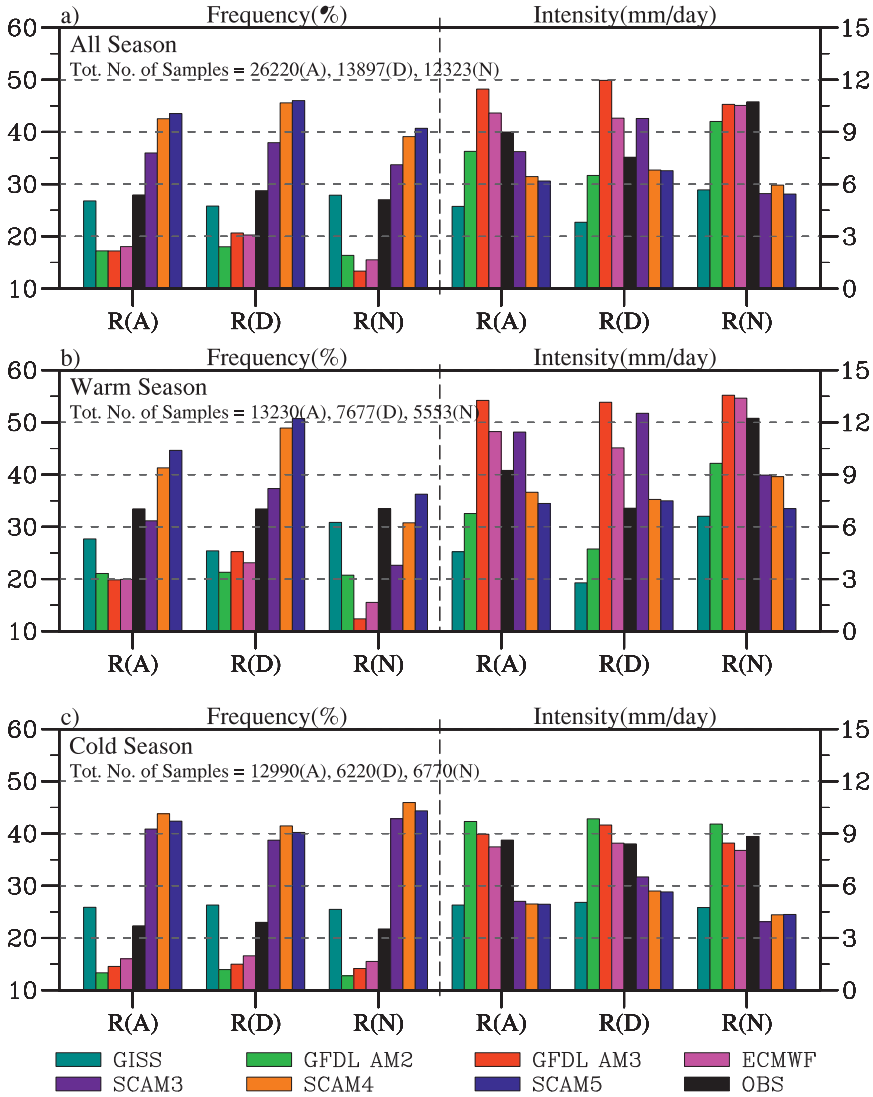

FIG. 3. Frequency (lhs y axis) and mean intensity (rhs y axis) of rain events (Pr > 0.1 mm day^{-1}) for (a) all season, (b) warm season, and (c) cold season.

compensation between the frequency and mean intensity of rain events to produce the same amount of precipitation. Evidently, the existence of compensating errors is best illustrated by Fig. 4d, which demonstrates that even for those events that all the SCMs simulate the total precipitation reasonably well (|model bias| < 5 mm day^{-1}), the apparent good precipitation simulations may result from error compensation between the total number and mean intensity of the rain events.

More detailed frequency distributions of the hourly precipitation intensity are shown in Fig. 5. Overall, the frequency of precipitation occurrence decreases with increasing precipitation intensity in both the observations and the models. The model bias characteristics, however, vary between different seasons and daytime or nighttime conditions. In the warm season, compared with the observations, the nighttime frequencies for moderate-to-strong precipitation (Pr > 5 mm day^{-1}) are lower for all models, while daytime frequencies for stronger precipitation are mostly higher except for the GISS-E2 and GFDL AM2 SCMs. The frequencies of light precipitation (Pr < 1 mm day^{-1}) in the warm season are higher only in GISS-E2 and SCAM5, which is true for both daytime and nighttime conditions. In the cold season, the light-to-moderate precipitation events (Pr < 5 mm day^{-1}) occur more frequently in both daytime and nighttime for GISS-E2 and the three SCAMs. The two GFDL and ECMWF SCMs have a lower frequency occurrence for the entire precipitation spectrum. In addition, in the daytime the GISS-E2 SCM has much

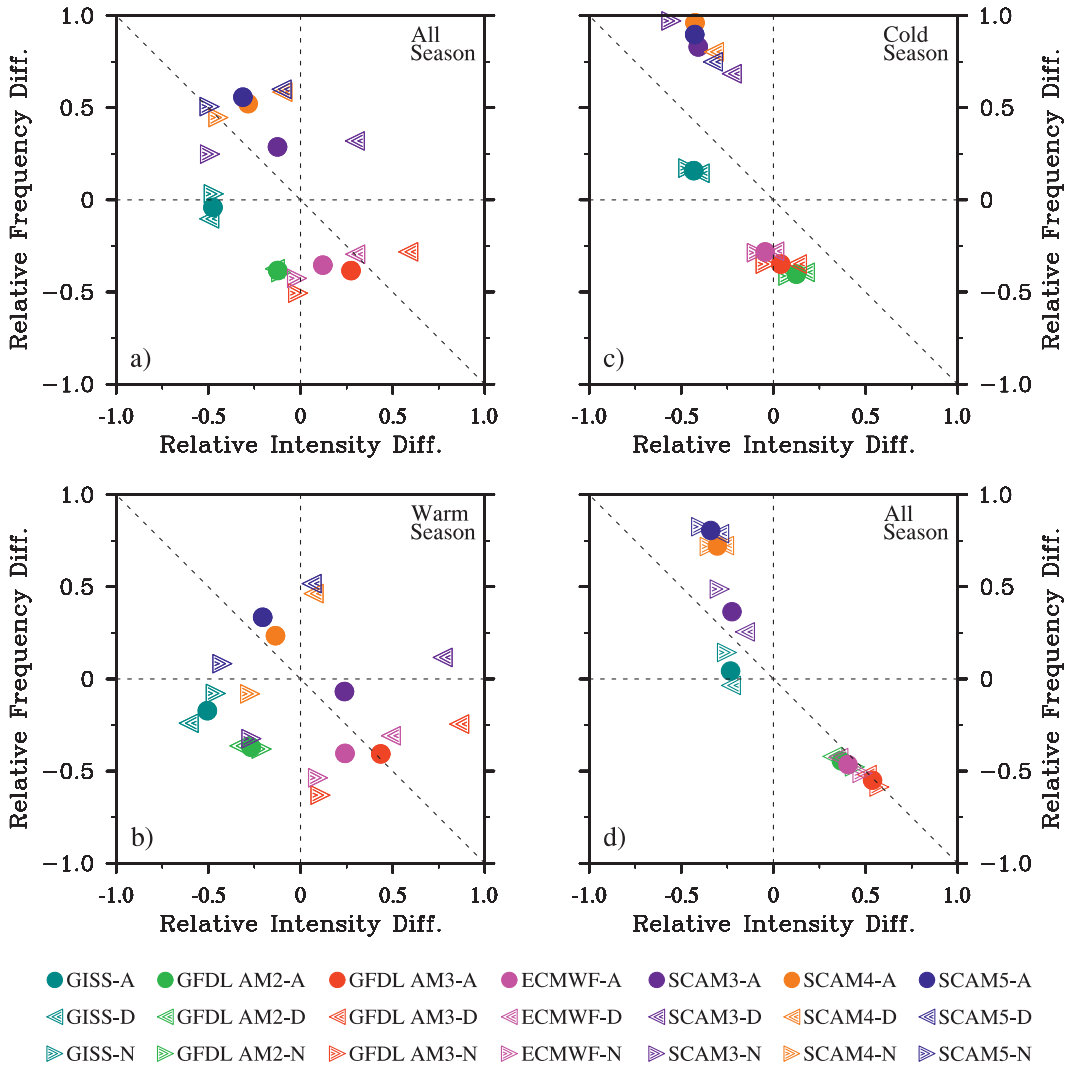

FIG. 4. Scatterplots of relative intensity difference and relative frequency difference of 7 SCMs for rain events (Pr > 0.1 mm day^{-1}) for (a) all season, (b) warm season, (c) cold season, and (d) all season with model bias in total precipitation (<5 mm day^{-1}). Relative intensity (frequency) difference is defined as the model intensity (frequency) bias normalized by the observed intensity (frequency) of rain events.

higher frequency of precipitation events stronger than 1 mm day^{-1} in the cold than warm season, while the observations and most other SCMs have a higher frequency of mild-to-strong precipitation events (stronger than 1 mm day^{-1} and weaker than 50 mm day^{-1}) in the warm than cold season. Another noteworthy point is that the frequency differences between each SCM and observations are smaller in the cold than warm season for strong precipitation events (Pr > 20 mm day^{-1}).

d. Partition between convective and stratiform precipitation

Modeled total precipitation is the sum of convective and stratiform precipitation from the convection scheme and large-scale macro-/microphysical schemes, respectively. Previous comparison studies showed that the intermodel difference in convective precipitation is generally larger than that in total and stratiform precipitation (Xie et al. 2005). To examine the relative contributions of convective and stratiform precipitating processes to the total precipitation biases, Fig. 6 shows ratios of the convective to total precipitation in the seven SCMs at each specified total precipitation range, for the warm and cold seasons, respectively. In general, the relative contribution to total precipitation by model convective process is larger during the warm season and more so in the daytime than in the nighttime to some extent, though in the observation, if the frequency of stronger precipitation is

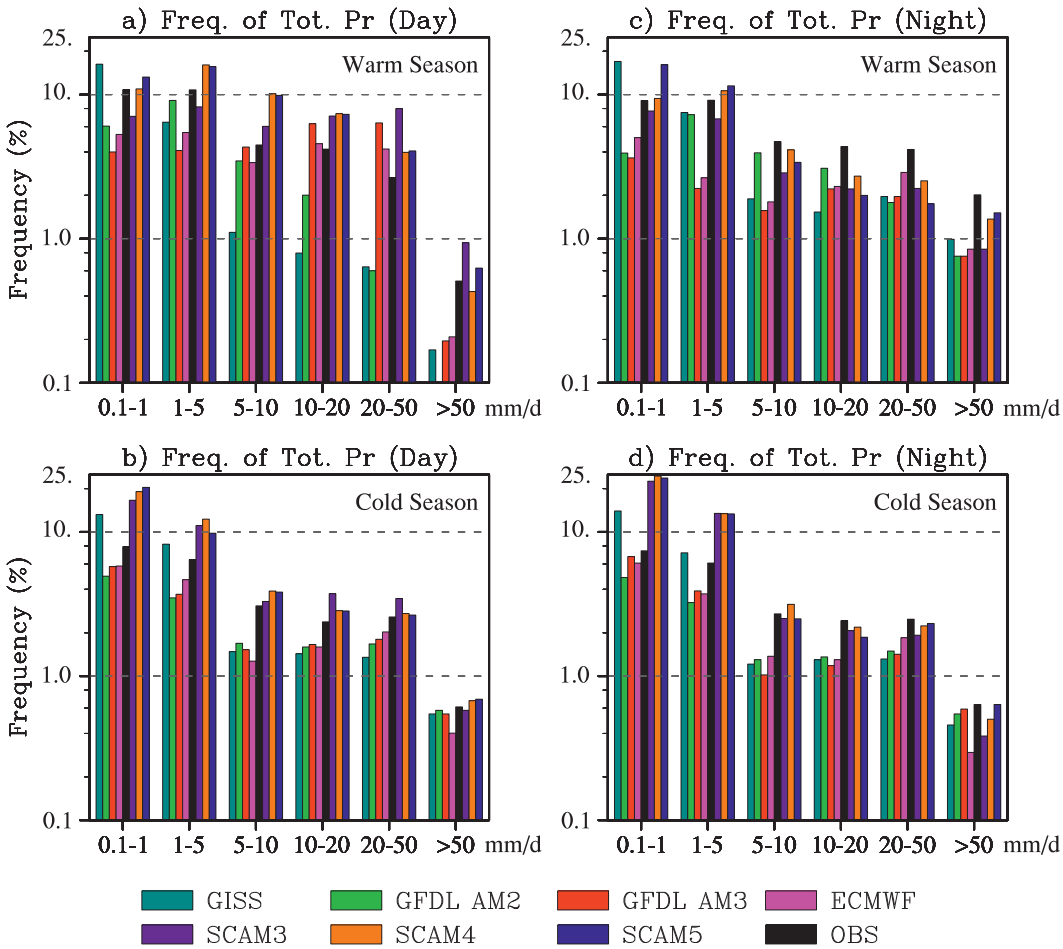

FIG. 5. Frequency of daytime total precipitation for the (a) warm and (b) cold seasons. Frequency of nighttime total precipitation for the (c) warm and (d) cold seasons.

any indication, there exists no such a tendency in either the warm or cold season.

It is also worth noting that the performances of the two GFDL SCMs are significantly different in that the AM2 SCM has much higher ratios of convective to total precipitation in the rain events weaker than 5 mm day^{-1}, while the AM3 SCM has much higher ratios of convective to total precipitation in the rain events stronger than 20 mm day^{-1}. The ratios of the convective to total precipitation in the three SCAMs are also quite different. The convective precipitation ratio is higher in SCAM3 and lower in SCAM5, especially in the nighttime. Other than GFDL AM2, the convective scheme in general has a relatively small role in light precipitation events, though the role is relatively larger for most models in the daytime and warm season. Under all conditions, the convection scheme in the GISS-E2 model plays a much smaller role, relative to the other six models, in producing total surface precipitation. This issue will be further discussed later in section 4a.

Figure 7 shows the frequency of convective precipitation events (convective precipitation intensity larger than 0.1 mm day^{-1}) in the seven SCMs at each specified total precipitation range, for the warm and cold seasons, respectively. Convective precipitation occurs more frequently in the daytime than in the nighttime for most SCMs, especially those with CAPE-based triggers. Events of convective precipitation are mainly with a total precipitation rate less than 50 mm day^{-1}. Another noticeable point is the occurrences of convective precipitation in GISS-E2 SCM are more frequent in the cold than warm season.

4. Further analyses

a. Relationship between precipitation and possible influencing factors

The above analysis shows that although most models can reproduce the observed total precipitation reasonably

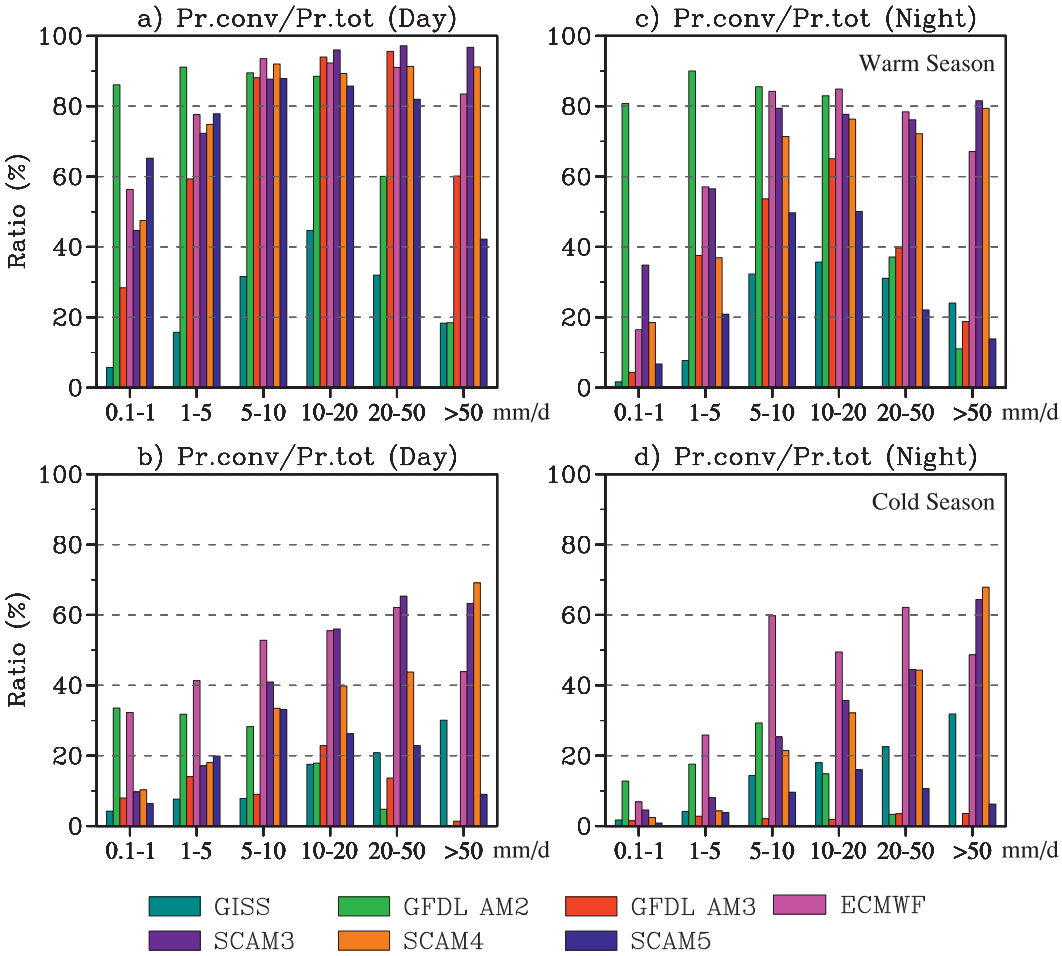

FIG. 6. Ratios of convective to total precipitation by each range of total precipitation in daytime for the (a) warm and (b) cold seasons, and in nighttime for the (c) warm and (d) cold seasons.

well, there are significant and interesting differences in their details. This section examines possible factors that likely influence the detailed model performances.

Figure 8 compares the relationships between the total precipitation and 500-hPa vertical pressure velocity for rain events only. Total precipitation is tightly coupled to the large-scale vertical motion in the observations, especially in the warm season (Figs. S1, S2 in the supplemental material). The warm season also has more frequent extreme upward motions and precipitation in nighttime than in daytime. Note that the close correlation between total precipitation and vertical motion likely arises from the fact that the vertical pressure velocity derives from the variational algorithm constrained by surface precipitation (Xie et al. 2004). However, these two quantities are much less tightly coupled in the models and the relationship differs in different SCMs. Relative to the observations, there exists a significant precipitation bias in most models when vertical motions are weak, and the bias occurs predominantly in the daytime (Figs. 9, 10) and in the warm season. It is interesting to note that GFDL AM3 SCM and SCAM3 still have some biases in the cold season. On average, the model coupling between total precipitation and large-scale vertical motion is stronger in the cold than warm season, even after excluding the large precipitation bias at the weak vertical-motion regime. It is worth emphasizing that this seasonal difference is completely opposite to that in the observations. Relative to the other models, the GISS-E2 and GFDL AM2 SCMs do not exhibit a significant precipitation bias in the weak vertical-motion regime (Fig. 9).

Strong precipitation in the model in the absence of substantial large-scale ascending motions is presumed to be caused by convection parameterizations. CAPE is the key ingredient in any cumulus convection. Figure 11 shows the joint probability distribution function (PDF) of CAPE and total precipitation for weak vertical-motion regimes ($|\omega_{500}| < 50$ hPa day^{-1}) in which the black

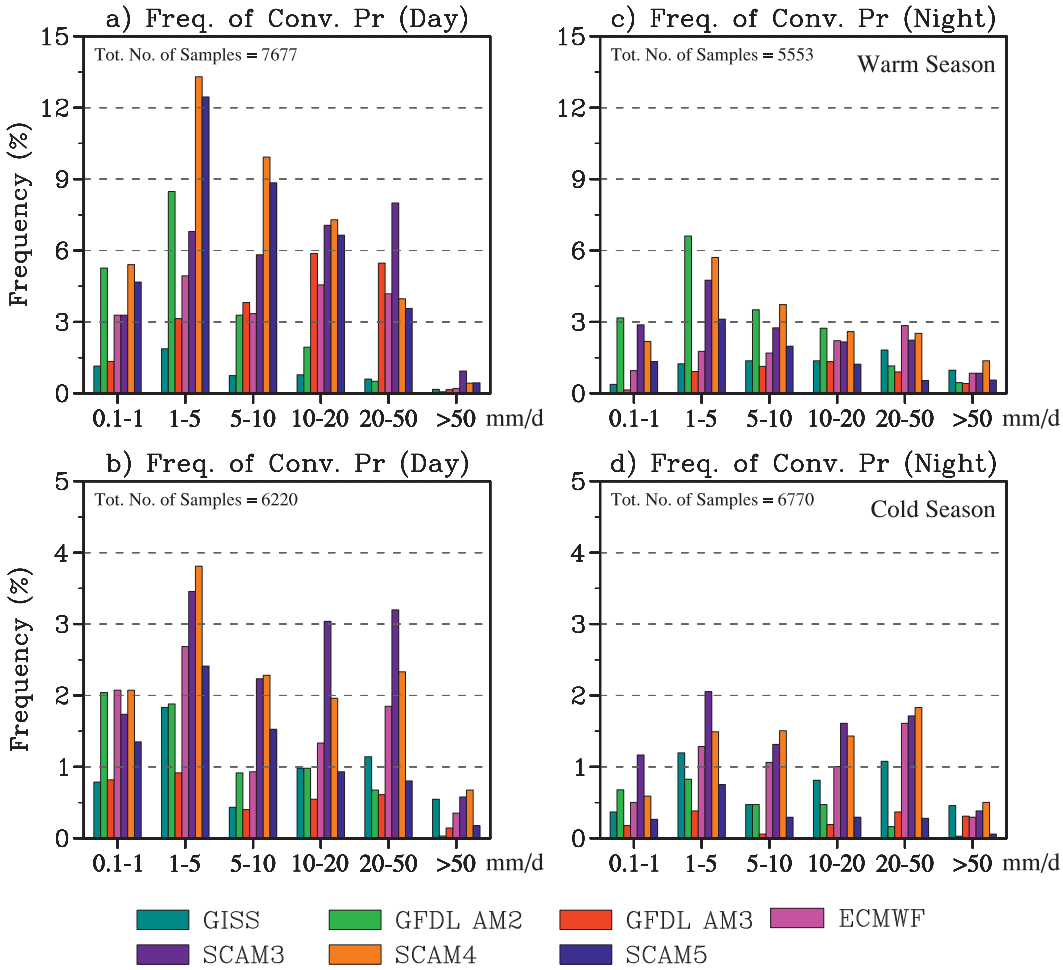

FIG. 7. Frequency of convective precipitation binned by each range of total precipitation in daytime for the (a) warm and (b) cold seasons, and in nighttime for the (c) warm and (d) cold seasons.

lines are the averaged total precipitation for each CAPE bin. In the observations weak precipitation can frequently occur in a broad range of CAPE with intensity slightly decreasing with increasing CAPE. The GISS-E2 SCM shows a similar pattern as the observation. In GFDL AM2 SCM, most events have a small total precipitation, which increases mildly with CAPE values. In other SCMs, especially GFDL AM3, ECMWF, and SCAM3, the occurrences of large CAPE are accompanied by a strong total precipitation. The total precipitation around the weak vertical-motion regimes stems mainly from the convective precipitation in SCMs (Fig. S3 in the supplemental material). Relative to SCAM3, the large precipitation biases and strong dependence of total precipitation on CAPE are markedly reduced in SCAM4 and SCAM5, with quite similar patterns. The similarity between SCAM4 and SCAM5 is understandable because the main difference between CAM4 and CAM3 is the deep convection scheme, whereas the CAM4 and CAM5 differ in all other parameterization schemes except the deep convection scheme. The major change from GFDL AM2 to AM3 is also the deep convection scheme. The significant differences in the joint PDFs between SCAM4, SCAM5, and SCAM3, as well as that between AM2 and AM3, suggest that the deep convection scheme is the main culprit for the model bias in producing the spurious strong precipitation around the weak vertical-motion regimes. Kennedy et al. (2011) showed that the continuous large-scale forcing data used in driving the SCM simulations have a moist bias in the boundary layer when compared with the ARM Climate Modeling Best Estimate (Xie et al. 2010) soundings. This moist bias likely influences the model convective precipitation, especially for SCMs with CAPE-based triggers. A moister boundary layer should yield higher CAPEs and likely leads to a higher frequency of convection. This will probably influence other convective parameterizations as well, such as reducing convective inhibition (CIN) and making

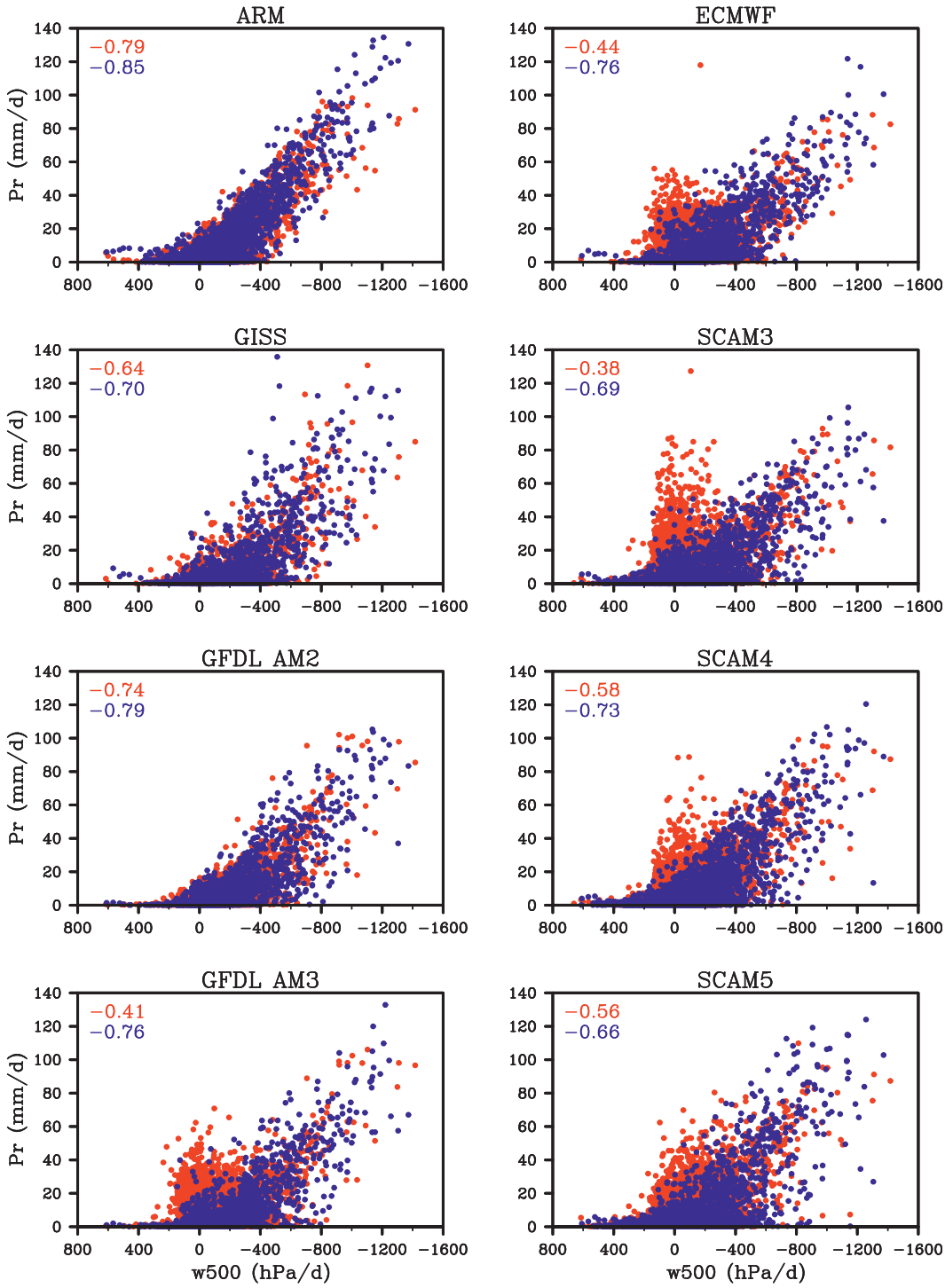

FIG. 8. Scatterplots of 500-hPa vertical pressure velocity (ω_{500}) and total precipitation for precipitation events only (Pr > 0.1 mm day^{-1}) in ARM observations and 7 SCMs for daytime (red dots) and nighttime (blue dots). Correlation coefficients between ω_{500} and total precipitation for daytime (red) and nighttime (blue) are marked in each panel.

parcel lifting easier. Although the influence of such moist biases in the boundary layer on model precipitation warrants further investigation, the large differences among the models in this weakly forced dynamical regime suggest that this influence is at most secondary relative to the convection parameterizations themselves.

Properties of PBL may also affect convective activity. A model with too shallow a PBL or too strong an inversion

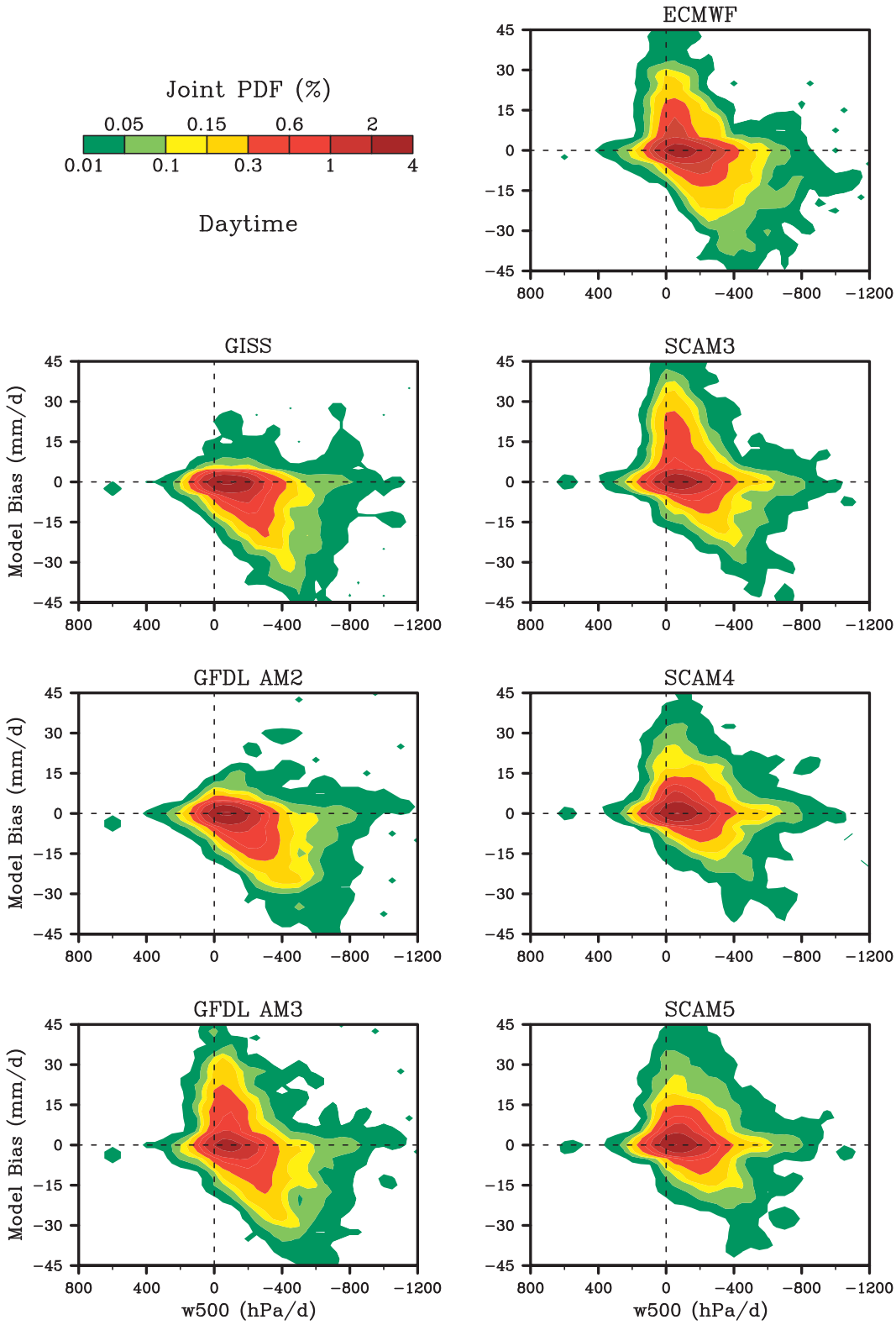

FIG. 9. Joint PDF binned by ω_{500} and model bias in total precipitation (Pr.SCM − Pr.Obs) for daytime precipitation events only (Pr > 0.1 mm day^{-1}) in 7 SCMs.

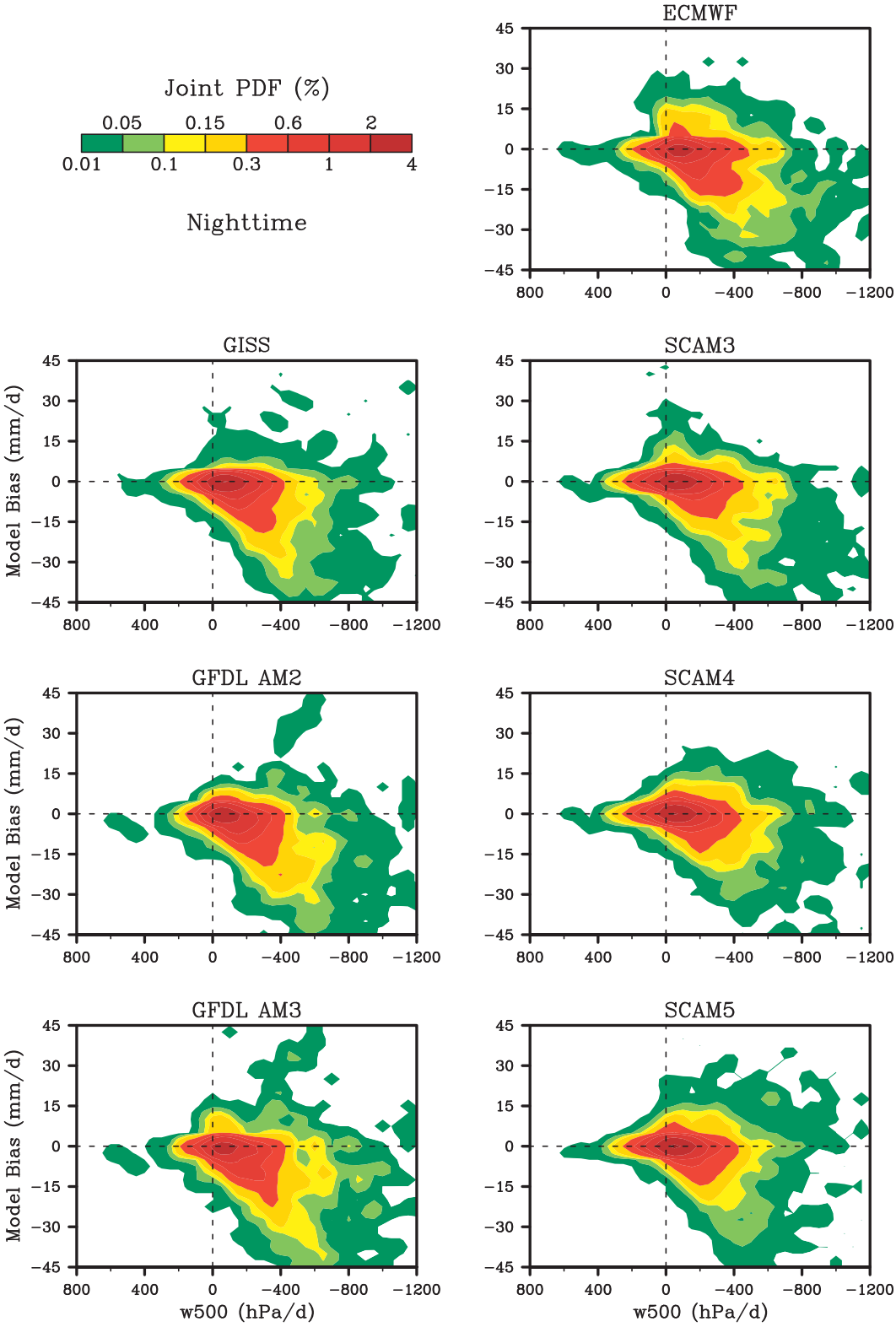

FIG. 10. As in Fig. 9, but for nighttime.

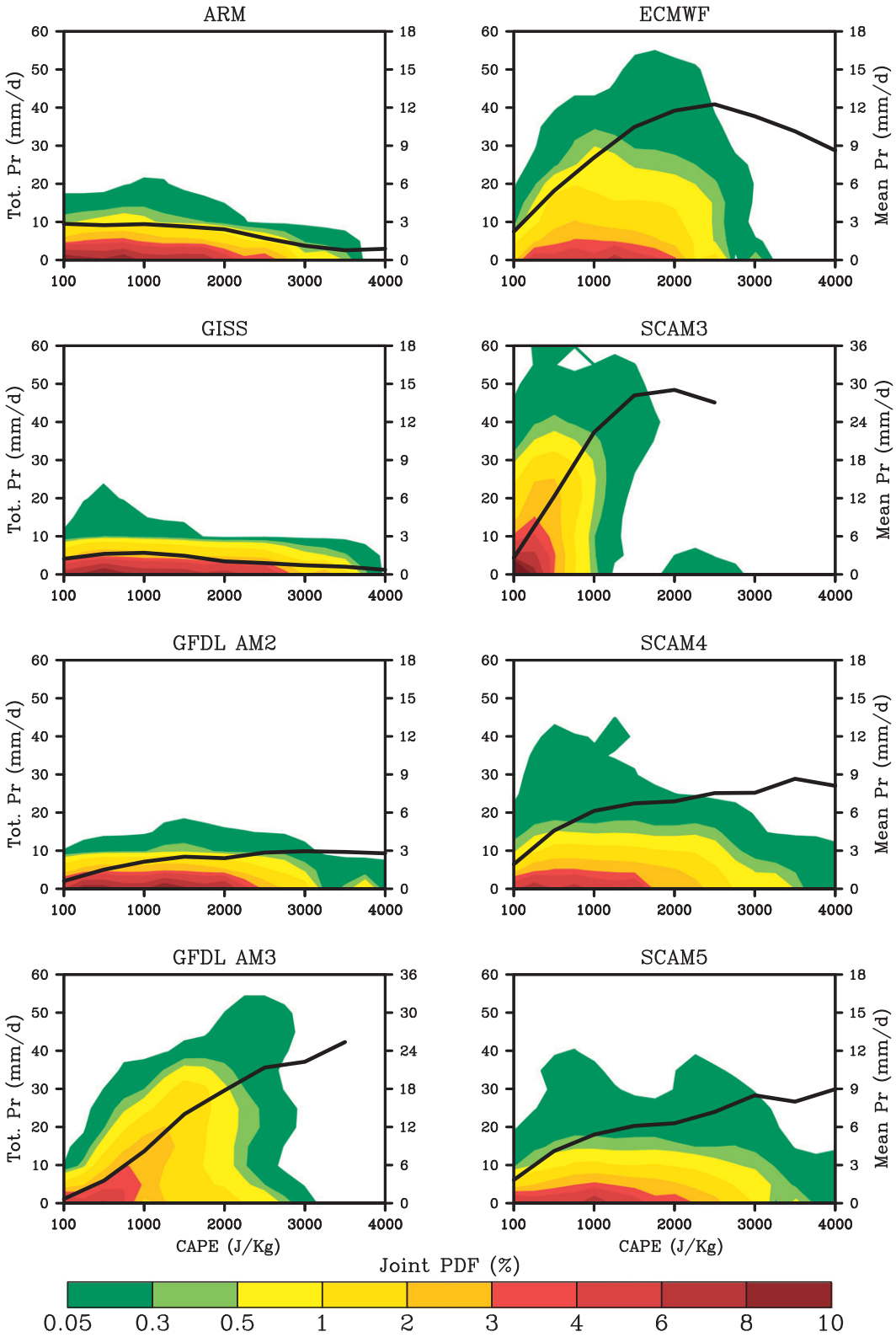

FIG. 11. Joint PDF (shaded) binned by CAPE and total precipitation and averaged total precipitation (black line) binned by CAPE for precipitation events only (Pr > 0.1 mm day^{-1}) in ARM observations and 7 SCMs when $|\omega_{500}| <$ 50 hPa day^{-1}.

TABLE 4. Correlation coefficients (cor.) between (top two rows) precipitation and CAPE, and (bottom two rows) between precipitation and PBL height, for $|\omega_{500}| < 50$ hPa day^{-1} [daytime (4939) and nighttime (4252)] events.

		Data							
Cor. of variables	Time	OBS	GISS-E2	GFDL AM2	GFDL AM3	ECMWF IFS	CAM3	CAM4	CAM5
Pr, CAPE	Day	0.01	−0.01	0.27	0.46	0.22	0.66	0.38	0.43
	Night	0.13	0.09	0.34	0.28	0.09	0.35	0.22	0.20
Pr, PBL_H	Day	−0.05	−0.07	−0.09	0.08	−0.03	−0.10	−0.05	−0.04
	Night	0.09	−0.07	0.15	0.09	−0.04	0.12	0.11	0.18

might not convect even if its cumulus parameterization was perfect. Previous studies (e.g., Hannay et al. 2009) showed that models shared a common problem of having a PBL depth too shallow relative to observations. Our examination of the SCM simulations confirms this finding (Fig. S4 in the supplemental material). The shallower PBL, which implies weaker turbulence and smaller turbulent kinetic energy (TKE), may indeed be a factor for the GISS-E2 SCM that uses parcel-lifting-based triggers for convection and exhibits weaker convective activities. However, the overly active convections in the other models, as mentioned above, suggest that the role played by PBL parameterization in this aspect, if any, is minor. It can be further confirmed by Table 4 that model precipitation has a much stronger dependence on the CAPE than the PBL height.

Bretherton et al. (2004b) showed a tight relationship between surface precipitation and precipitable water (vertically integrated specific humidity) over the tropical oceanic regions using satellite data, and suggested that such a relationship can provide a useful constraint on the parameterization of tropical deep convection. To see if there is a certain relationship between the two variables in the observations over midlatitude land and how well the models capture this relationship, we analyze and compare the relationships between precipitation and precipitable water (PW) at the ARM SGP site in the observations and seven SCMs. Figure 12 depicts the averaged total, stratiform, and convective precipitation binned by PW in the daytime and nighttime. Total precipitation rates increase with PW in both the observations and the SCMs. However, the increase of precipitation with increasing PW is off beyond PW $\sim$ 20 mm in the observations in the daytime, whereas GFDL AM3, ECMWF, and SCAMs do not capture this behavior. It is mainly caused by the excessive precipitation from their convection schemes. Again the models have a better agreement with the observations in the nighttime. The primary contributor to the relationship is the convection-induced precipitation except for the GISS-E2 SCM and SCAM5, whose stratiform schemes play larger roles in accounting for this relationship. For the GISS-E2 model, as also reported in Kennedy (2011), this is likely because a little bit of convection detrains lots of water for the stratiform scheme to consume, or the stratiform scheme produces clouds/precipitation in response to large vertical motions in the forcing.

To further investigate how the 500-hPa vertical-pressure velocity and PW are related to precipitation, the joint PDF of 500-hPa vertical pressure velocity and PW is shown in Fig. 13, along with the averaged total precipitation intensity for each joint bin. It is clear that the most frequent events occur around the weaker vertical-motion regimes with PW ranging from 10 to 50 mm. The frequency peak with larger PW occurs in the warm season and with smaller PW occurs in the cold season (Figs. S5, S6 in the supplemental material). On the other hand, PW also increases with the strengthening ascending velocity. In the observations, the increase of the averaged total precipitation intensity mostly coincides with the increasing vertical velocity, while in most SCMs, except for the GISS-E2 and GFDL AM2 SCMs, a stronger influence of PW is evident indicated by the tilting of isopleths of 5 and 10 mm day^{-1} around the weak vertical-motion regimes, especially in the daytime (Figs. S7, S8 in the supplemental material). This may be one of the reasons that the model precipitation is not coupled with the large-scale vertical motion as tightly as the observations shown in Fig. 8. The stronger dependence of modeled precipitation on the PW is mostly because of the treatment of the convective process, which is illustrated in Fig. 12. The value of PW measures the total available water vapor in the whole air column; another moisture variable that is better related to condensation and conversion to precipitation is the air column relative humidity (RH). The joint PDF for the column-averaged RH and PW in the weak vertical-motion regimes (magnitudes of vertical pressure velocity are smaller than 50 hPa day^{-1}), and the averaged total precipitation for each joint bin are shown in Fig. 14. The joint PDF demonstrates that the most frequent events are associated with a column RH of about 50% and PW of about 40 mm in the observations and most SCMs. The precipitation intensity is quite small in the observations for all joint bins, while in most

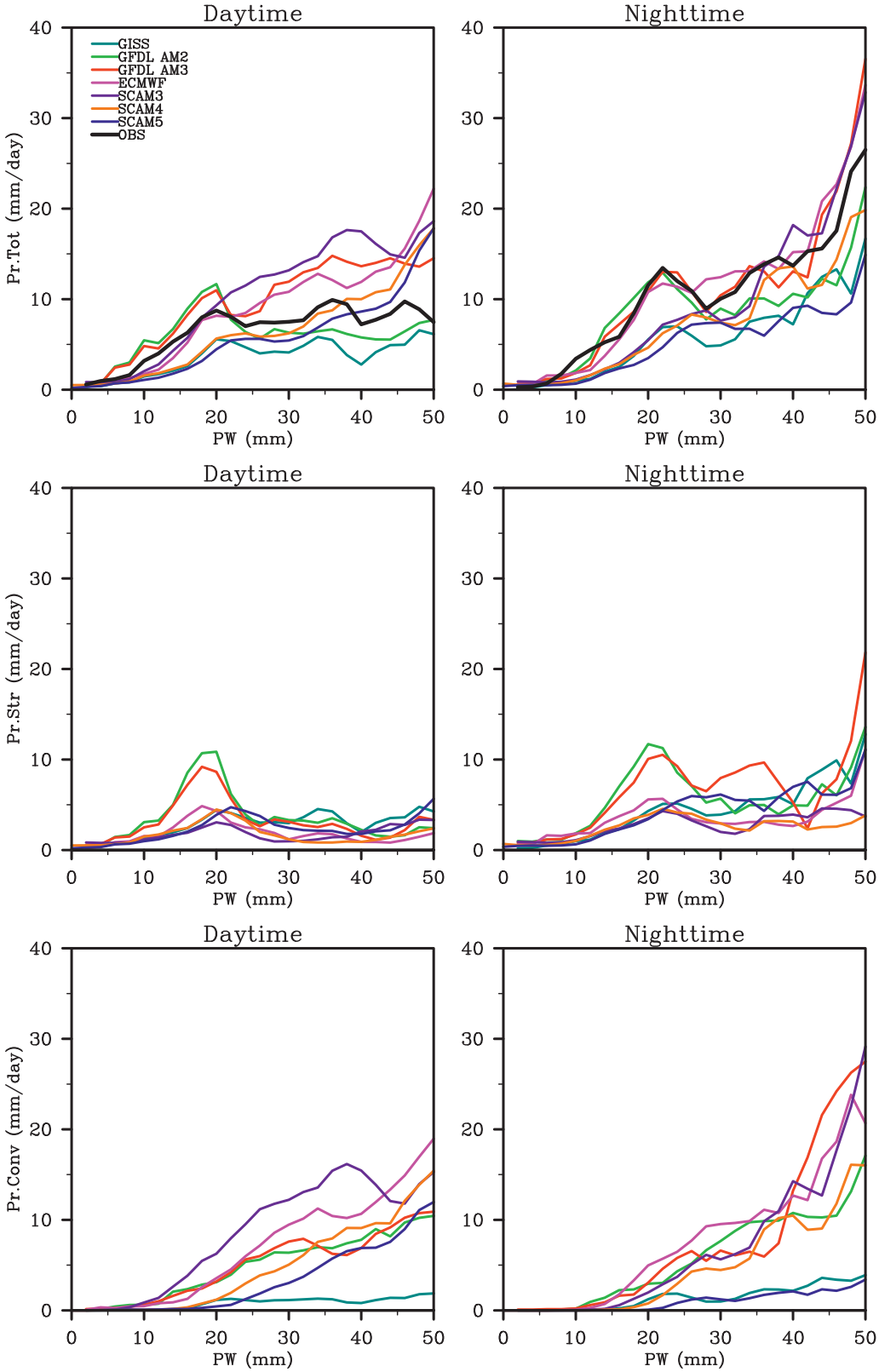

FIG. 12. Averaged total precipitation, stratiform precipitation, and convective precipitation binned by PW for (left) daytime and (right) nighttime precipitation events (Pr > 0.1 mm day^{-1}).

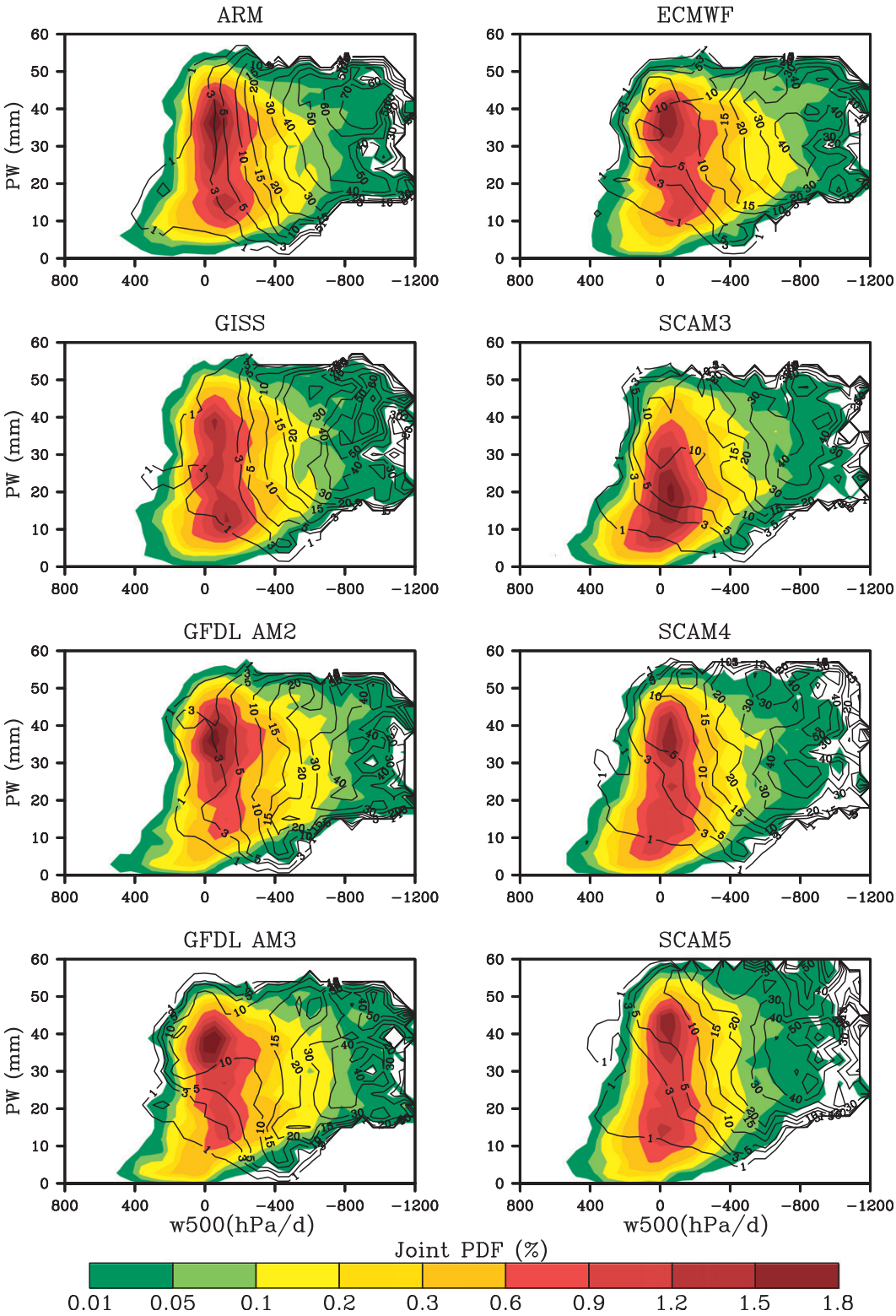

FIG. 13. Joint PDF (shaded) and averaged total precipitation (contours) binned by ω_{500} and PW for precipitation events only (Pr > 0.1 mm day^{-1}) in ARM observations and 7 SCMs.

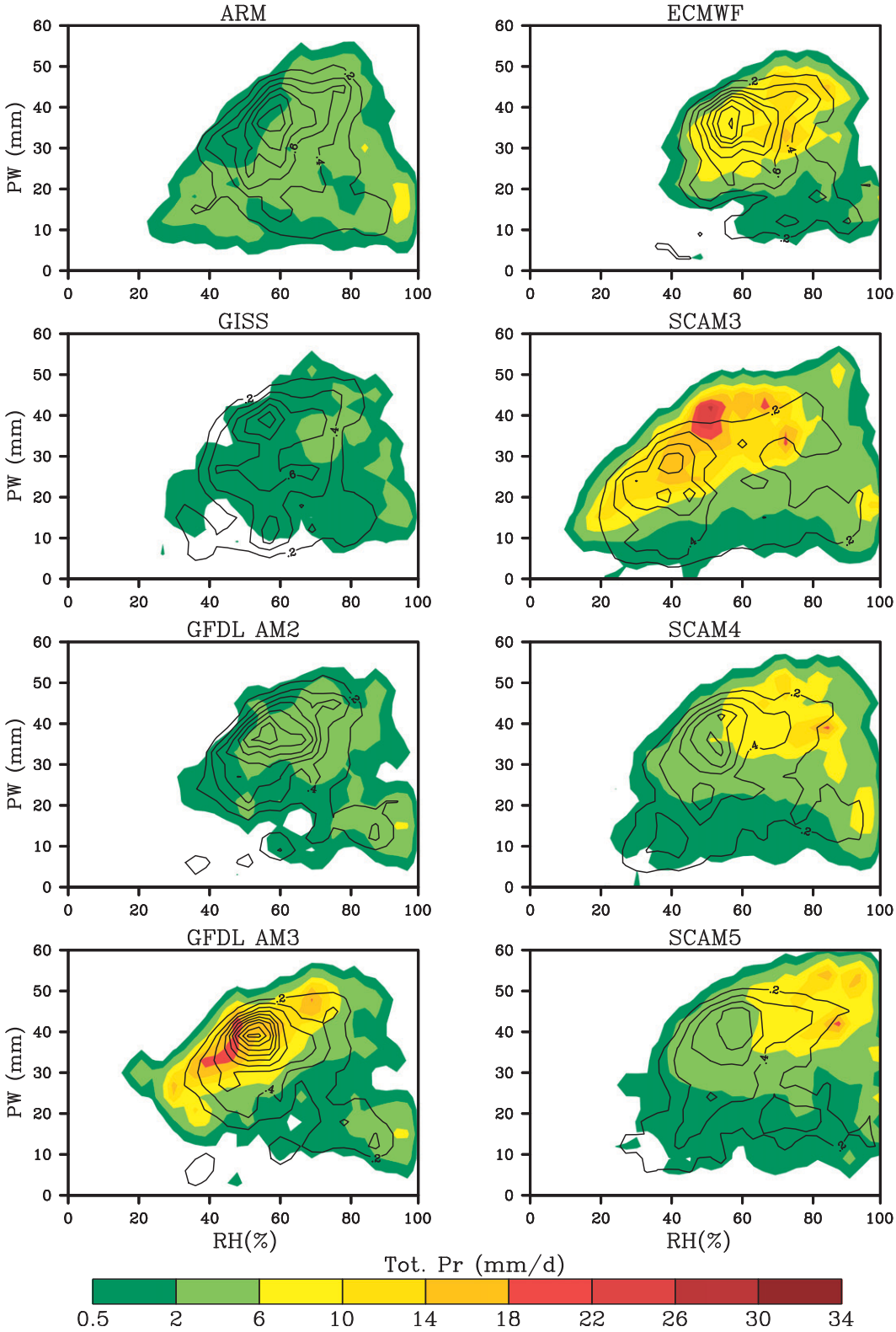

FIG. 14. Averaged total precipitation (shaded) and joint PDF (contours) binned by RH and PW for precipitation events only (Pr > 0.1 mm day^{-1}) in ARM observations and 7 SCMs when $|\omega_{500}| < 50$ hPa day^{-1}.

SCMs there is some intense rain in the events with large RH and PW, which is mostly contributed by the convective precipitation (Fig. 15) in the daytime (Figs. S9, S10 in the supplemental material).

The analysis in this section shows that 1) the large difference between the observed and SCM-simulated precipitation is mainly around the weak vertical-motion regime. This spurious precipitation bias produced by most SCMs has a strong dependence on the CAPE, which is true especially for those models with deep convection parameterizations using CAPE-based triggers. 2) Most SCMs produce strong precipitation (mainly from convective precipitation) when there are large PW and RH around the weak dynamical regimes, which is not seen in the observations. This difference implies that the observed surface precipitation at the SGP site is mainly controlled by large-scale vertical uplift, while the production of precipitation in most of the models from the cumulus/stratiform schemes is also significantly affected by the handling of convective triggers.

b. *Analysis of extreme events*

To further pin down the conditions under which the models tend to underestimate or overestimate the observed precipitation, this section focuses on a number of special events with substantial precipitation biases. Particularly interesting are the two extreme categories of events: 1) all the SCMs underestimate the observed precipitation more than 20 mm day^{-1}, and 2) most SCMs overestimate the observed precipitation more than 10 mm day^{-1} (the events that SCMs overestimate the observed precipitation more than 20 mm day^{-1} are very few in the nighttime). Note that since there are very few overestimate events in the GISS-E2 and GFDL AM2 SCMs (Fig. 2), there are no events that all the SCMs overestimate the observed precipitation simultaneously.

Figure 16 compares the total precipitation and convective precipitation rates for the two categories, in daytime and nighttime. For the category whereby all the SCMs underestimate precipitation (38 events in daytime and 69 events in nighttime), the total precipitation rates in the seven SCMs are quite similar in both daytime and nighttime, all being much weaker than the observation. For the category whereby some models overestimate by more than 10 mm day^{-1} (36 events in daytime and 4 events in nighttime), the events occur when the observations have weak (daytime) or moderate (nighttime) precipitation. The convective precipitation rates are excessively large in most SCMs in the daytime.

Figure 17 further compares the profiles of averaged vertical pressure velocity, horizontal thermal advection, horizontal moisture advection, and surface LH and SH fluxes in the large-scale forcing data for the two categories of events. For the model underestimation events, the large-scale meteorological backgrounds in the daytime and the nighttime are quite similar, with strong upward motions, weak horizontal thermal advection, and negative low-level horizontal moisture advection. For the model overestimation events, in the daytime there are weak vertical motions while in the nighttime there are moderate upward motions. There are strong positive low-level horizontal thermal advection, weak negative mid-to-high-level thermal advection, and strong positive low-level horizontal moisture advection in both the daytime and nighttime with much stronger intensity in the nighttime. In the daytime there are very strong surface LH and SH fluxes, providing sufficient moisture supplies. The low-level warm and moist air convergence builds up a favorable condition for most SCMs (especially those with CAPE-triggered convection) to produce strong convective precipitation, especially in the daytime.

The results from this section highlight the dependence of model performance on large-scale environments. The model underestimation events occur in the strong ascending regimes with negative low-level horizontal heat and moisture advection. The model overestimation events occur in the weak (in the daytime) or moderate (in the nighttime) ascending regimes with positive low-level horizontal heat and moisture advection. Moisture is supplied mainly by the surface evaporation in the daytime and by the positive horizontal moisture advection in the nighttime for model overestimation events. While the overestimation events are clearly related to overactive convective activities and have stronger dependence on the CAPE in the models, it is much less clear why those large underestimation events occur when ascending conditions are strong and the observations actually record substantial precipitations. One possible reason is that the observed precipitation is short-lived; a slight time shift in the models may cause them to miss the major precipitation event at the observed time. Another possible reason is that the large-scale forcings, as shown in Fig. 17, tend to reduce CAPE and increase CIN making convection in the models less likely to be triggered, while the observed may indeed be convective in nature and triggered by other mechanisms. There is also a possibility that the majority of the precipitating hydrometeors are advected into the column in the observations, instead of locally generated. The models lack such hydrometeor sources because large-scale forcings of hydrometeors are not available from the observations.

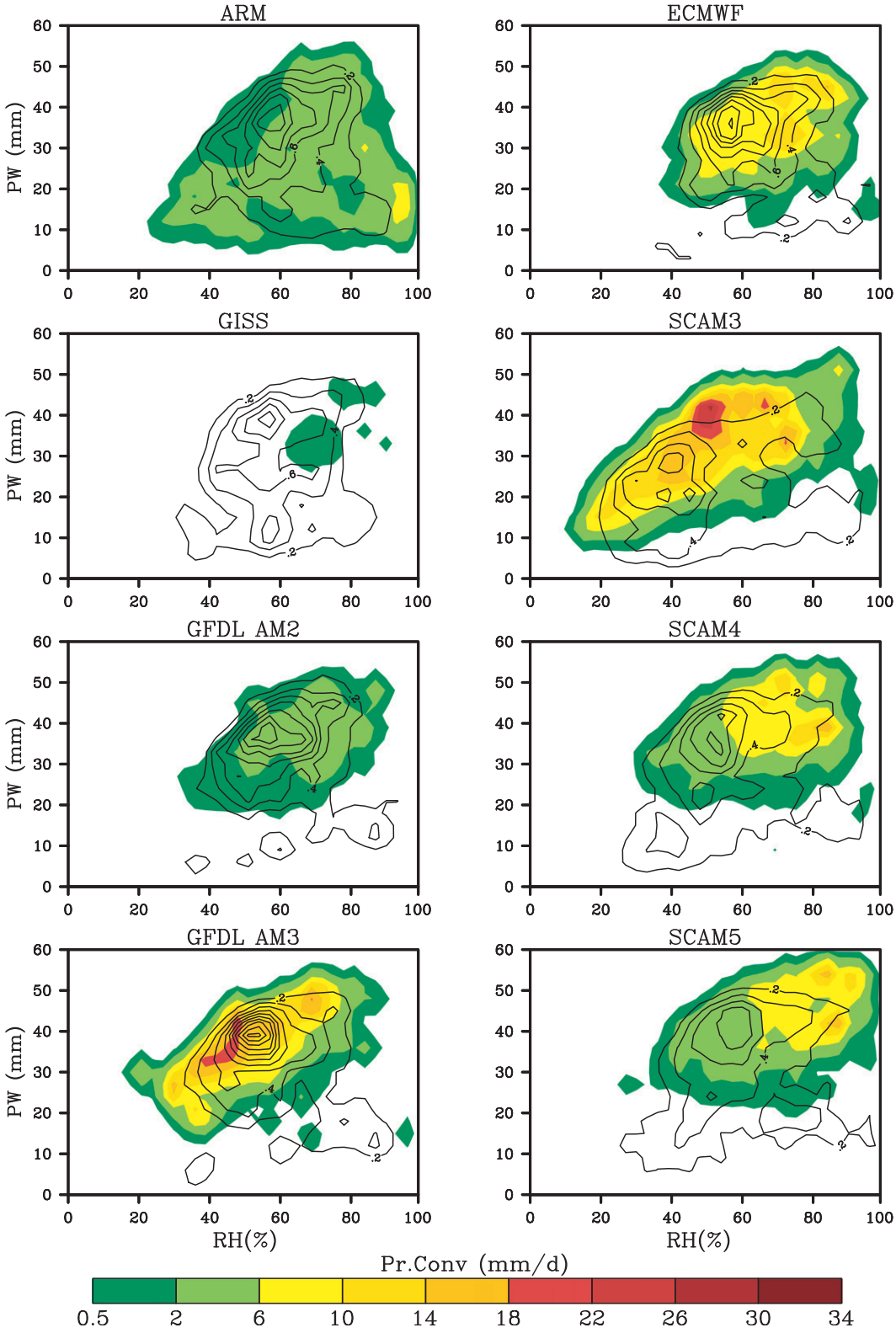

FIG. 15. As in Fig. 14, except for convective precipitation in 7 SCMs and total precipitation in ARM observations.

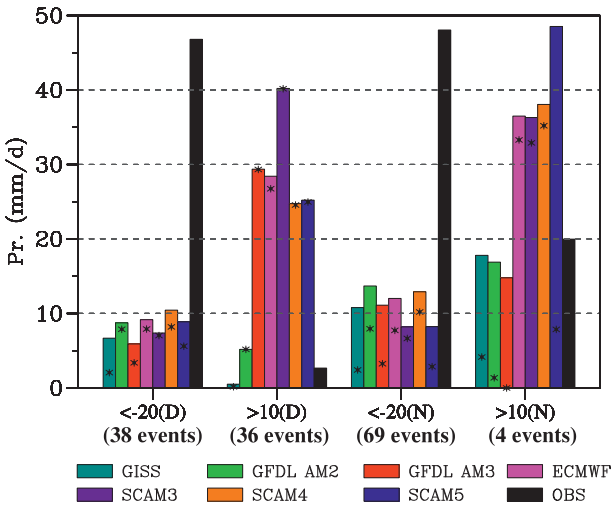

FIG. 16. Averaged total precipitation amounts in 7 SCMs and ARM observations for events with total precipitation difference (dPr) < -20 mm day^{-1} for all the SCMs, dPr > 10 mm day^{-1} for certain SCMs in the daytime (indicated by D) and nighttime (indicated by N). The dPr is defined as Pr in SCM minus Pr in Obs. Asterisks represent the averaged convective precipitation amounts in 7 SCMs.

5. Summary

This study quantitatively evaluates the statistical performances of the seven SCMs by comparing simulated precipitation with observations from 1999–2001 at the ARM SGP site. The 3-yr-long evaluation permits improved statistical evaluation of many aspects. It is found that although most SCMs can reproduce the observed total precipitation reasonably well, there are significant and interesting differences in their details, including differences between daytime and nighttime, between the warm and cold seasons, between frequency and mean precipitation intensity, and between convective and stratiform partition. First, in the warm season, most SCMs produce more rain events in the daytime than in the nighttime while the observations have more rain events in the nighttime. The mean intensities of rain events in most SCMs are much stronger (weaker) in the daytime (nighttime) than the observations. In the cold seasons, the model–observation differences in the frequency and mean intensity of rain events tend to compensate each other for most SCMs. In the daytime, most SCMs have a higher frequency of moderate-to-strong precipitation events (10–50 mm day^{-1}) than the observations in the warm season. In the nighttime, all the SCMs have lower frequency of moderate-to-strong precipitation events (>10 mm day^{-1}) than the observations for both the warm and cold seasons. Even for the precipitation events that all the SCMs simulate the total precipitation well, different SCMs achieve the good performance by different combinations of compensating errors between the number of precipitation events and the mean precipitation intensity.

Second, the higher frequency of warm-season daytime precipitation events in most SCMs is related to the fact that most SCMs produce a spurious precipitation peak around the regime of weak vertical motions. The spurious precipitation peak is mainly produced by the strong convective precipitation when precipitable water and relative humidity are large. This spurious precipitation bias has strong dependence on the CAPE, especially for those models with deep convection parameterizations using CAPE-based triggers.

Third, analyses of extreme events reveal distinct meteorological backgrounds for model underestimation and overestimation events. The model underestimation events occur in the strong ascending regimes with negative low-level horizontal heat and moisture advection, whereas model overestimation events occur in the weak (in the daytime) or moderate (in the nighttime) ascending regimes with positive low-level horizontal heat and moisture advection. Moisture is supplied mainly by surface evaporation in the daytime and by the positive horizontal moisture advection in the nighttime for model overestimation events.

The different SCM performances and associations with large-scale forcing and thermodynamic factors shed useful insights on convection parameterizations and future development as well. For example, the analysis also reveals that the convective precipitation is much weaker in the GISS-E2 SCM (Figs. 6, 12). According to Del Genio and Wolf (2012), the weaker convective precipitation may be related to the parcel-lifting-based trigger used in the convection scheme. The GISS-E2 SCM often cannot convect under the observed thermodynamic structure at the time the observed precipitation begins because the turbulent kinetic energy is not strong enough to provide updrafts to lift the air parcel to the level of free convection against large CIN within one time step. On the other hand, the models using CAPE-based triggers can produce convective precipitation even under large CIN. However, there is no observational support for such CAPE-based triggers (Jakob et al. 2011). Moreover, the relevant forcing for many convective situations at the SGP site is mesoscale in nature and is thus absent or inaccurately represented in both the forcing and the parameterizations themselves (Del Genio et al. 2012). Whether the SCM with today's cumulus parameterizations, which are forced with the large-scale information and parameterize only cloud-scale response to that forcing, should convect at the SGP site is still an open question. More investigation is in order along this line.

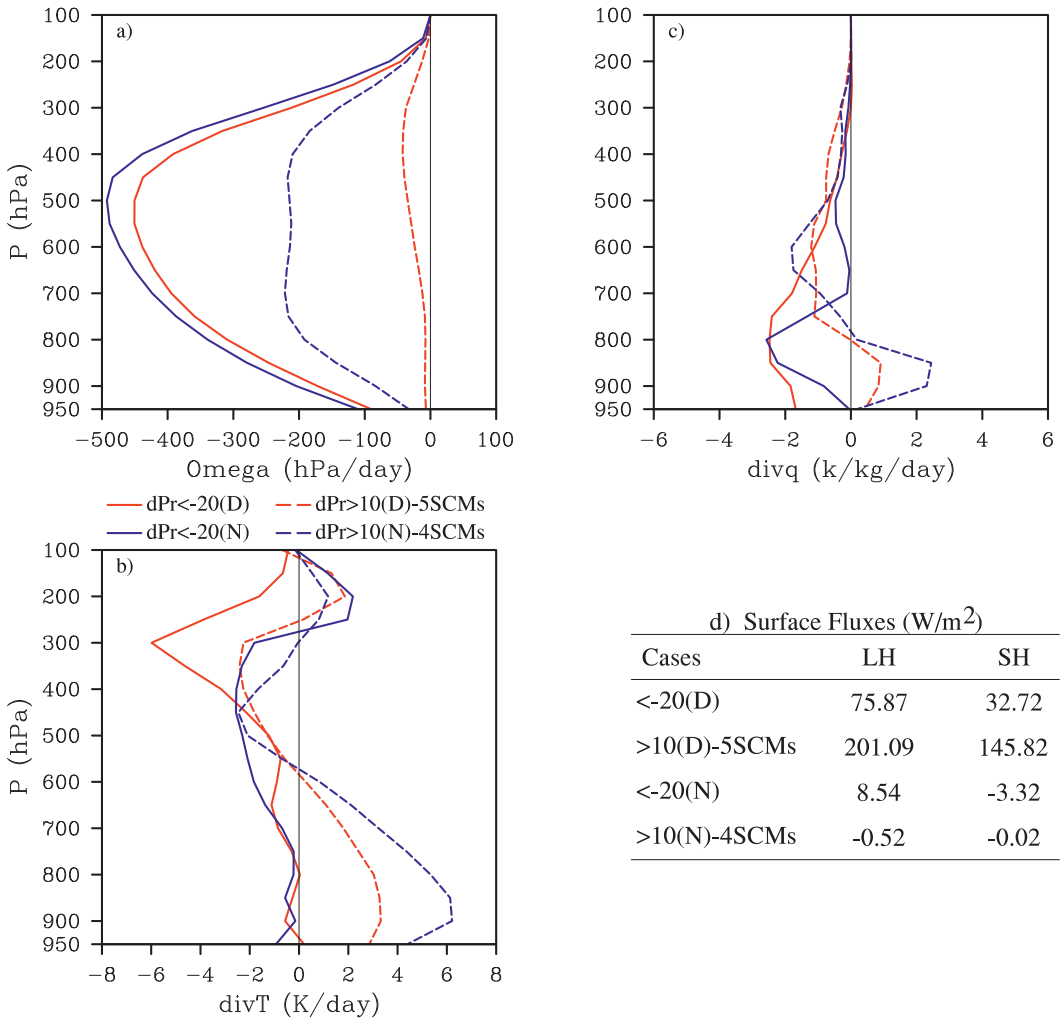

d) Surface Fluxes (W/m^2)

Cases	LH	SH
<-20(D)	75.87	32.72
>10(D)-5SCMs	201.09	145.82
<-20(N)	8.54	-3.32
>10(N)-4SCMs	-0.52	-0.02

FIG. 17. Vertical profiles of (a) averaged vertical pressure velocity, (b) horizontal T advection, (c) horizontal q advection, and (d) averaged surface fluxes in the large-scale continuous forcing data for events with dPr < -20 mm day^{-1} for all the SCMs, dPr > 10 mm day^{-1} for certain SCMs in the daytime and nighttime.

Acknowledgments. This work is part of the FASTER project (http://www.bnl.gov/faster/) supported by the U.S. Department of Energy Earth System Modeling (ESM) program. The authors thank the two anonymous reviewers for their constructive comments. The first author also would like to express her sincere gratitude to her former advisor Dr. Minghua Zhang for his incessant support and encouragement throughout her research.

REFERENCES

Ackerman, T. P., and G. M. Stokes, 2003: The Atmospheric Radiation Measurement Program. *Phys. Today,* **56,** 39–44.

Arakawa, A., and W. H. Schubert, 1974: Interaction of a cumulus cloud ensemble with the large-scale environment, Part I. *J. Atmos. Sci.,* **31,** 674–701.

Bechtold, P., and Coauthors, 2004: The simulation of the diurnal cycle of convective precipitation over land in a global model. *Quart. J. Roy. Meteor. Soc.,* **130,** 3119–3137.

Betts, A. K., and C. Jakob, 2002: Study of diurnal cycle of convective precipitation over Amazonia using a single column model. *J. Geophys. Res.,* **107,** 4732, doi:10.1029/2002JD002264.

Bretherton, C. S., and S. Park, 2009: A new moist turbulence parameterization in the Community Atmosphere Model. *J. Climate,* **22,** 3422–3448.

——, J. R. McCaa, and H. Grenier, 2004a: A new parameterization for shallow cumulus convection and its application to marine subtropical cloud-topped boundary layers. Part I: Description and 1D results. *Mon. Wea. Rev.,* **132,** 864–882.

——, M. E. Peters, and L. E. Back, 2004b: Relationships between water vapor path and precipitation over the tropical oceans. *J. Climate,* **17,** 1517–1528.

Dai, A., 2006: Precipitation characteristics in eighteen coupled climate models. *J. Climate,* **19,** 4605–4630.

——, and K. E. Trenberth, 2004: The diurnal cycle and its depiction in the Community Climate System Model. *J. Climate,* **17,** 930–951.

Del Genio, A. D., and M. Yao, 1993: Efficient cumulus parameterization for long-term climate studies: The GISS scheme.

The Representation of Cumulus Convection in Numerical Models, Meteor. Monogr., No. 46, Amer. Meteor. Soc., 181–184.

——, and A. Wolf, 2012: Should today's SCMs convect at the SGP? *FASTER Breakout, ASR Science Team Meeting,* Arlington, VA, Department of Energy, 11 pp. [Available online at http://asr.science.energy.gov/meetings/stm/2012/presentations/delgeniofaster.pdf.]

——, M.-S. Yao, W. Kovari, and K. K.-W. Lo, 1996: A prognostic cloud water parameterization for global climate models. *J. Climate,* **9,** 270–304.

——, W. Kovari, M.-S. Yao, and J. Jonas, 2005: Cumulus microphysics and climate sensitivity. *J. Climate,* **18,** 2376–2387.

——, M.-S. Yao, and J. Jonas, 2007: Will moist convection be stronger in a warmer climate? *Geophys. Res. Lett.,* **34,** L16703, doi:10.1029/2007GL030525.

——, J. Wu, and Y. Chen, 2012: Characteristics of mesoscale organization in WRF simulations of convection during TWP-ICE. *J. Climate,* **25,** 5666–5688.

Donner, L. J., C. J. Seman, R. S. Hemiler, and S. Fan, 2001: A cumulus parameterization including mass fluxes, convective vertical velocities, and mesoscale effects: Thermodynamic and hydrological aspects in a general circulation model. *J. Climate,* **14,** 3444–3463.

——, and Coauthors, 2011: The dynamical core, physical parameterizations, and basic simulation characteristics of the atmospheric component AM3 of the GFDL global coupled model CM3. *J. Climate,* **24,** 3484–3519.

Ghan, S. J., X. Bian, and L. Corsetti, 1996: Simulation of the Great Plains low-level jet and associated clouds by general circulation models. *Mon. Wea. Rev.,* **124,** 1388–1408.

——, L. R. Leung, and J. McCaa, 1999: A comparison of three different modeling strategies for evaluating cloud and radiation parameterizations. *Mon. Wea. Rev.,* **127,** 1967–1984.

——, and Coauthors, 2000: An intercomparison of single column model simulations of summertime midlatitude continental convection. *J. Geophys. Res.,* **105,** 2091–2124.

Gregory, D., J.-J. Morcrette, C. Jakob, A. M. Beljaars, and T. Stockdale, 2000: Revision of convection, radiation and cloud schemes in the ECMWF Integrated Forecasting System. *Quart. J. Roy. Meteor. Soc.,* **126,** 1686–1710.

Hack, J. J., 1994: Parameterization of moist convection in the National Center for Atmospheric Research Community Climate Model (CCM2). *J. Geophys. Res.,* **99** (D3), 5551–5568.

——, and J. A. Pedretti, 2000: Assessment of solution uncertainties in single-column modeling frameworks. *J. Climate,* **13,** 352–365.

Hannay, C., and Coauthors, 2009: Evaluation of forecasted southeast Pacific stratocumulus in the NCAR, GFDL, and ECMWF models. *J. Climate,* **22,** 2871–2889.

Holtslag, A. A. M., and B. A. Boville, 1993: Local versus nonlocal boundary layer diffusion in a global climate model. *J. Climate,* **6,** 1825–1842.

Jakob, C., L. Davies, V. Kumar, and P. May, 2011: Representing convection in models—How stochastic does it need to be? *Proc. ECMWF Workshop on Representing Model Uncertainty and Error in Weather and Climate Prediction,* Reading, United Kingdom, ECMWF, 41–52.

Kennedy, A. D., 2011: Evaluation of a single column model at the southern Great Plains climate research facility. Ph.D. dissertation, University of North Dakota, 149 pp.

——, and Coauthors, 2010: Evaluation of the NASA GISS single column model simulated clouds using combined surface and satellite observations. *J. Climate,* **23,** 5175–5192.

——, X. Dong, B. Xi, S. Xie, Y. Zhang, and J. Chen, 2011: A comparison of MERRA and NARR reanalyses with the DOE ARM SGP data. *J. Climate,* **24,** 4541–4557.

Köhler, M., 2005: Improved prediction of boundary layer clouds. *ECMWF Newsletter,* No. 104, ECMWF, Reading, United Kingdom, 18–22.

Lee, M.-I., and S. D. Schubert, 2008: The diurnal cycle in NASA's Modern Era Retrospective-Analysis for Research and Applications (MERRA). Preprints, *20th Conf. Climate Variability and Change,* New Orleans, LA, Amer. Meteor. Soc., P3.7. [Available online at https://ams.confex.com/ams/88Annual/techprogram/paper_134706.htm.]

——, and Coauthors, 2007: An analysis of the warm-season diurnal cycle over the continental United States and northern Mexico in general circulation models. *J. Hydrometeor.,* **8,** 344–366.

——, and Coauthors, 2008: Role of convection triggers in the simulation of the diurnal cycle of precipitation over the United States Great Plains in a general circulation model. *J. Geophys. Res.,* **113,** D02111, doi:10.1029/2007JD008984.

Lin, J.-L., 2007: The double-ITCZ problem in IPCC AR4 coupled GCMs: Ocean–atmosphere feedback analysis. *J. Climate,* **20,** 4497–4525.

Liu, G., Y. Liu, and S. Endo, 2013: Evaluation of surface flux parameterization with long-term ARM observations. *Mon. Wea. Rev.,* **141,** 773–797.

Lock, A. P., A. R. Brown, M. R. Bush, G. M. Martin, and R. N. B. Smith, 2000: A new boundary layer mixing scheme. Part I: Scheme description and single-column model tests. *Mon. Wea. Rev.,* **128,** 3187–3199.

Moorthi, S., and M. J. Suarez, 1992: Relaxed Arakawa–Schubert: A parameterization of moist convection for general circulation models. *Mon. Wea. Rev.,* **120,** 978–1002.

Morrison, H., and A. Gettelman, 2008: A new two-moment bulk stratiform cloud microphysics scheme in the Community Atmospheric Model (CAM3). Part I: Description and numerical tests. *J. Climate,* **21,** 3845–3862.

Neale, R. B., J. H. Richter, and M. Jochum, 2008: The impact of convection on ENSO: From a delayed oscillator to a series of events. *J. Climate,* **21,** 5904–5924.

Neggers, R. A. J., A. P. Siebesma, and T. Heus, 2012: Continuous single-column model evaluation at a permanent meteorological supersite. *Bull. Amer. Meteor. Soc.,* **93,** 1389–1400.

Park, S., and C. S. Bretherton, 2009: The University of Washington shallow convection and moist turbulence schemes and their impact on climate simulations with the Community Atmosphere Model. *J. Climate,* **22,** 3449–3469.

Randall, D., and D. G. Cripe, 1999: Alternative methods for specification of observed forcing in single-column models and cloud system models. *J. Geophys. Res.,* **104** (D20), 24 527–24 545.

——, and Coauthors, 2003: Confronting models with data: The GEWEX Cloud Systems Study. *Bull. Amer. Meteor. Soc.,* **84,** 455–469.

Rasch, P. J., and J. E. Kristjansson, 1998: A comparison of the CCM3 model climate using diagnosed and predicted condensate parameterizations. *J. Climate,* **11,** 1587–1614.

Rotstayn, L. D., 1997: A physical based scheme for the treatment of stratiform clouds and precipitation in large-scale models. I: Description and evaluation of the microphysical processes. *Quart. J. Roy. Meteor. Soc.,* **123,** 1227–1282.

Schmidt, G. A., and Coauthors, 2006: Present-day atmospheric simulations using GISS ModelE: Comparison to in situ, satellite, and reanalysis data. *J. Climate,* **19,** 153–192.

Stokes, G. M., and S. E. Schwartz, 1994: The Atmospheric Radiation Measurement (ARM) program: Programmatic background and design of the cloud and radiation testbed. *Bull. Amer. Meteor. Soc.,* **75,** 1201–1221.

Sun, Y., S. Solomon, A. Dai, and R. W. Portmann, 2006: How often does it rain? *J. Climate,* **19,** 916–934.

Tiedtke, M., 1989: A comprehensive mass flux scheme for cumulus parameterization in large-scale models. *Mon. Wea. Rev.,* **117,** 1779–1800.

——, 1993: Representation of clouds in large-scale models. *Mon. Wea. Rev.,* **121,** 3040–3061.

Wu, W., Y. Liu, and A. K. Betts, 2012: Observationally based evaluation of NWP reanalyses in modeling cloud properties over the southern Great Plains. *J. Geophys. Res.,* **117,** D12202, doi:10.1029/2011JD016971.

Xie, S., and M. Zhang, 2000: Impact of the convection trigger function on single-column model simulations. *J. Geophys. Res.,* **105** (D11), 14 983–14 996.

——, and Coauthors, 2002: Intercomparison and evaluation of cumulus parameterizations under summertime midlatitude continental conditions. *Quart. J. Roy. Meteor. Soc.,* **128,** 1095–1135.

——, R. T. Cederwall, and M. Zhang, 2004: Developing long-term single-column model/cloud system–resolving model forcing data using numerical weather prediction products constrained by surface and top of atmosphere observations. *J. Geophys. Res.,* **109,** D01104, doi:10.1029/2003JD004045.

——, and Coauthors, 2005: Simulations of midlatitude frontal clouds by single-column and cloud-resolving models during the Atmospheric Radiation Measurement March 2000 cloud intensive operational period. *J. Geophys. Res.,* **110,** D15S03, doi:10.1029/2004JD005119.

——, and Coauthors, 2010: Cloud and more: ARM climate modeling best estimate data. *Bull. Amer. Meteor. Soc.,* **91,** 13–20.

Zhang, G. J., 2003: Roles of tropospheric and boundary layer forcing in the diurnal cycle of convection in the U.S. southern Great Plains. *Geophys. Res. Lett.,* **30,** 2281, doi:10.1029/2003GL018554.

——, and N. A. McFarlane, 1995: Sensitivity of climate simulations to the parameterization of cumulus convection in the Canadian Climate Center general circulation model. *Atmos.–Ocean,* **33,** 407–446.

Zhang, M., W. Lin, C. S. Bretherton, J. J. Hack, and P. J. Rasch, 2003: A modified formulation of fractional stratiform condensation rate in the NCAR Community Atmospheric Model (CAM2). *J. Geophys. Res.,* **108,** 4035, doi:10.1029/2002JD002523.

Zhao, M., I. M. Held, S.-J. Lin, and G. A. Vecchi, 2009: Simulations of global hurricane climatology, interannual variability, and response to global warming using a 50-km resolution GCM. *J. Climate,* **22,** 6653–6678.